CHI3L1 drives astrocyte-medicated neuronal injury via GAL3-NLRP3 signaling in ischemic stroke

Haiyan Li
Third Affiliated Hospital of Sun Yat-sen University
Ying Deng
Southern Medical University
Jinan Chen
Third Affiliated Hospital of Sun Yat-sen University
Yubao Lu
Third Affiliated Hospital of Sun Yat-sen University
Yinyao Lin
Third Affiliated Hospital of Sun Yat-sen University
Xuejiao Men
Third Affiliated Hospital of Sun Yat-sen University
Yuyan Zeng
Tsinghua University
Haoyang Li
Beijing Tian Tan Hospital
Guangyou Wang
First Affiliated Hospital of Harbin Medical University
Yu-Wen Alvin Huang
Brown University
Bingjun Zhang
Third Affiliated Hospital of Sun Yat-sen University
Ziqi Liang
Nanjing University
Da Mi
Tsinghua University
Xuan Li
Harbin Medical University Cancer Hospital
Changyong Tang
tangchy23@mail.sysu.edu.cn

Third Affiliated Hospital of Sun Yat-sen University

Research Article

Keywords: CHI3L1 proteins, GAL3 receptors, NLRP3 inflammasomes, ischemic strokes, astrocytes, neuronal injuries

Posted Date: June 2nd, 2026

DOI: https://doi.org/10.21203/rs.3.rs-9462748/v1

Additional Declarations: No competing interests reported.

CHI3L1 drives astrocyte-medicated neuronal injury via GAL3-NLRP3 signaling in ischemic stroke

Haiyan Li [1†], Ying Deng [1,2*†], Jinan Chen[1], Yubao Lu [1], Yinyao Lin[1], Xuejiao Men[1], Yuyan Zeng[3], Haoyang Li[4], Guangyou Wang[5], Yu-Wen Alvin Huang[6], Bingjun Zhang[1], Ziqi Liang[8], Da Mi[3*], Xuan Li[7*], Changyong Tang[1*]

[1*]Department of Neurology, The Third Affiliated Hospital of Sun Yat-Sen University, No. 600 Tianhe Road, Guangzhou, 510630, Guangdong Province, China.
[2]School of Traditional Chinese Medicine , Southern Medical University, No. 1023 South Shatai Road, Guangzhou, 510515, Guangdong Province, China.
[3]State Key Laboratory of Membrane Biology, IDG/McGovern Institute for Brain Research, Tsinghua-Peking Joint Centre for Life Sciences, School of Life Sciences, Tsinghua University, Beijing , 100084, China.
[4]Department of Neurology, Beijing Tiantan Hospital, Capital Medical University, Beijing, 100070, China.
[5]Department of Neurology, First Affiliated Clinical Hospital of Harbin Medical University, Harbin, 150081, China.
[6]Department of Molecular Biology, Cell Biology, and Biochemistry, Brown University, 70 Ship Street, Providence, RI 02903, USA.
[7]Department of Anesthesiology, Harbin Medical University Cancer Hospital, Harbin Medical University, Harbin, 150081, China.
[8]Institute of Modern Biology, Nanjing University, No. 163 Xianlin Avenue, Nanjing, 210008, Jiangsu, China.

*Corresponding author(s). E-mail(s): dy1994@sina.com ; mida@mail.tsinghua.edu.cn; lixuan@hrbmu.edu.cn; tangchy23@mail.sysu.edu.cn ;
Contributing authors: lihaiyan4159@163.com; chen20010514@126.com; luyb8@mail2.sysu.edu.cn; linyinyao@126.com; mxuejiao@mail.sysu.edu.cn; zeng-yy20@mails.tsinghua.edu.cn;

lhy881121@163.com; wangguangyou@hrbmu.edu.cn;
alvinhuang@brown.edu; gdbingjun@163.com; 837701371@qq.com;
†These authors contributed equally to this work.

Abstract

Background: Ischemic stroke lacks effective therapies. Whether chitinase-3-like protein 1 (CHI3L1) is involved in astrocyte-mediated neuronal injury, and its regulatory mechanism in both patient serum and ischemic brain tissue, remain largely unknown.**Methods:** We combined clinical proteomics, mouse tMCAO, in vitro OGD models, and genetic/pharmacological interventions to define CHI3L1 expression, function and downstream signaling.**Results:** CHI3L1 is robustly elevated in stroke patient serum and astrocytes in peri-infarct brain, correlating with stroke severity. CHI3L1 aggravates neuronal apoptosis, BBB disruption and functional deficits by activating GAL3–NLRP3 inflammasome. Astrocyte-specific GAL3 silencing or GB1107 inhibition markedly mitigates ischemic injury.**Conclusion:** The CHI3L1–GAL3–NLRP3 axis drives astrocyte-mediated neuronal damage in ischemic stroke, representing a promising therapeutic target.

Keywords: CHI3L1 proteins, GAL3 receptors,NLRP3 inflammasomes, ischemic strokes, astrocytes, neuronal injuries

1 Introduction

Stroke remains a major global health burden, contributing significantly to mortality and long-term disability [1, 2]. Ischemic stroke, which accounts for most cases, results from an abrupt interruption of cerebral blood flow, initiating a complex cascade of pathological events including energy failure, excitotoxicity, oxidative stress, and a strong inflammatory response [1, 3–5]. Simultaneously, the blood-brain barrier (BBB) is compromised, which is leading to widespread neuronal death and tissue infarction [6]. Despite extensive research efforts over the past decades, effective therapeutic interventions remain limited, highlighting a substantial unfulfilled clinical demand for solutions.

Among the many molecular players implicated in stroke pathophysiology, chitinase-3-like protein 1 (CHI3L1), also known as YKL-40, has emerged as a molecule of interest. CHI3L1 is a highly conserved glycoprotein that involved in various biological processes, including tissue remodeling, angiogenesis, and regulation of neuroinflammation. Increasing evidence has reported elevated CHI3L1 levels across a range of neurological disorders, such as traumatic brain injury (TBI), Alzheimer's disease (AD), Parkinson's disease (PD), amyotrophic lateral sclerosis (ALS), Creutzfeldt-Jakob disease (CJD), and multiple sclerosis (MS) [7–12]. Although initial studies have suggested a potential role for CHI3L1 in stroke, the molecular mechanisms underlying its involvement remain incompletely understood.

Our data showed that CHI3L1 was markedly upregulated in the peri-infarct region of the ischemic hemisphere, where it was largely co-expressed with the astrocytic

marker GFAP. These findings are consistent with single-cell RNA sequencing data from the Gene Expression Omnibus (GEO) database, where independent studies using C57BL/6J mouse brains subjected to transient middle cerebral artery occlusion (tMCAO) surgery also identified astrocyte-specific CHI3L1 elevation, supporting its potential relevance to stroke pathology [13, 14].

CHI3L1 seems to affect the behavior of microglia and astrocytes, both of which play central roles in the brain's innate immune response. After neurological injury, these glial cells become activated and release pro-inflammatory cytokines and chemokines, which can worsen inflammation and lead to additional neuronal damage [15–18]. CHI3L1 may influence neuroinflammatory responses by modulating the polarization and function of microglia and astrocytes. In models of traumatic brain injury (TBI), CHI3L1 has been shown to promote M1-type microglial activation, thereby enhancing pro-inflammatory signaling [10, 16, 19–21]. Additionally, CHI3L1 engages with several membrane receptors, including interleukin-13 receptor $\alpha 2$ (IL-13Rα2), Transmembrane Protein 219 (TMEM219), galectin-3 (GAL3), Chemoattractant receptor homologous molecule of Th2 cells (CRTH2), and CD44 activating downstream pathways such as AKT, β-catenin, and NF-κB. Disruption of these pathways has been associated with various neurological disorders [22–25]. Clinically, CHI3L1 levels are elevated in both serum and cerebrospinal fluid (CSF) of stroke patients [26–28]. For example, Rathcke et al. reported that higher serum YKL-40 levels were linked to increased mortality risk following ischemic stroke [29]. Elevated CHI3L1 concentrations in CSF have also been observed in patients with acute disseminated encephalomyelitis, neuromyelitis optica, and in subsets of multiple sclerosis patients with extensive radiological activity [30, 31]. In multiple sclerosis, a disease sharing some pathophysiological features with stroke, CHI3L1 has been linked to low-grade non-lymphocytic inflammation and active neurodegeneration, suggesting a broader role in disease progression [8, 32].

2 Results

2.1 Multi - modal Investigation Unveils CHI3L1 as a Key Player in Acute Ischemic Stroke Pathophysiology

Prior studies have reported elevated CHI3L1 expression in stroke patients (Table S1). To validate these findings, we performed proteomic sequencing of serum samples from 24 acute ischemic stroke (AIS) patients and age-matched controls (Table S2). Our analysis identified 355 proteins with altered expression, among which 164, including CHI3L1, were upregulated (**Fig. 1A–1B**). A heatmap visually depicted the differentially expressed proteins (**Fig. S1A**). KEGG pathway enrichment analysis revealed significant enrichment of the NLRP3 signaling pathway, along with other key pathways including MAPK, PI3K-Akt, and TNF signaling (**Fig. S1B**).

Subsequent ELISA assays confirmed a significant elevation of CHI3L1 levels in AIS patients (427.1 ± 212.5 ng/ml) compared to controls (197.6 ± 30.8 ng/ml, $p < 0.0001$) (**Fig. 1C; Table S3**). Furthermore, CHI3L1 levels positively correlated with both admission NIHSS scores (**Fig. 1D**), reflecting stroke severity, and infarct volume (**Fig.**

1E). These results reinforce the potential role of CHI3L1 in acute ischemic stroke pathophysiology.

In summary, our data not only replicates previous reports of increased CHI3L1 levels in stroke patients [16, 27, 29, 33]but also expands current knowledge by identifying additional upregulated proteins and related signaling pathways. The observed strong correlations involving CHI3L1 suggest its utility as a potential biomarker. They also provide a basis for further exploration of its role in stroke mechanisms and clinical applications. The temporal profile of CHI3L1 upregulation in peri-infarct brain regions and its robust elevation in patient serum samples—correlating with both stroke severity and infarct volume—positions CHI3L1 as not only a molecular effector but also a measurable proxy for disease burden. This dual significance reinforces its diagnostic and mechanistic relevance in stroke.

Despite the growing association between CHI3L1 and stroke, it's *in vivo* dynamics and functional implications have remained poorly defined. Given the significant burden of stroke, a more comprehensive understanding of the molecular mechanisms is critical for the development of effective therapies. Therefore, we investigated CHI3L1 expression in glial cells using tMCAO mouse model.

Immunostaining was employed to assess the expression of GFAP (astrocyte marker), IBA-1 (microglial marker), and CHI3L1 across key brain regions. These included the cortex, lateral ventricle, and peri-infarct area (**Fig. 1F; Fig. S1C**). Comparison of the affected and unaffected hemispheres revealed a marked upregulation of CHI3L1 in the ischemic regions, indicating its involvement in the brain's response to ischemic injury. Co-localization analysis revealed that only a small subset of microglia co-expressed CHI3L1, primarily near the infarct core, whereas the differential co-expression of CHI3L1 and GFAP between the two hemispheres was most pronounced in the peri-infarct region. Notably, a stronger overlap was observed between CHI3L1 and GFAP, indicating predominant upregulation in astrocytes.

Complementing our in vivo findings, we investigated CHI3L1 expression using an in vitro oxygen-glucose deprivation (OGD) model (**Fig. S1D**). Immunofluorescence staining of GFAP and CHI3L1 in primary astrocyte cultures demonstrated that cells subjected to 6 hours of OGD followed by 24 hours of reoxygenation (OGD6h-Re24h) exhibited significantly enhanced CHI3L1 secretion. This was in comparison to non-OGD controls (NON-OGD-Re). This *in vitro* evidence supports and strengthens our *in vivo* observations. Additionally, independent single-cell RNA sequencing data from the Gene Expression Omnibus (GEO) confirmed astrocyte-specific upregulation of CHI3L1 following cerebral ischemia in C57BL/6J mouse brains (**Fig. S2**).

To characterize the temporal dynamics of CHI3L1 expression, we monitored its levels in the cerebral cortex of tMCAO mice at multiple time points post-injury (**Fig. 1G**). CHI3L1 expression gradually increased between 6 hours and 3 days post-tMCAO, peaked between 3 and 7 days, and subsequently declined.

To complement qualitative observations with quantitative data, we performed Western blotting to assess CHI3L1 protein levels in the ischemic hemisphere at different time points (**Fig. 1H**). These results quantitatively confirmed the temporal upregulation of CHI3L1 following stroke, reinforcing the findings from immunostaining analyses.

To further confirm the temporal dynamics of CHI3L1 elevation in both brain tissue and serum following tMCAO, we performed sensitive ELISA analyses on samples from tMCAO mice. The results showed that CHI3L1 levels in brain tissue began to differ from those in normal tissue approximately 12 hours post-injury, with the most pronounced increase observed between 3 and 7 days, consistent with the findings from immunostaining and Western blotting (**Fig. S1E**). In contrast, CHI3L1 levels in serum displayed an earlier peak, rising between 1 and 3 days post-injury before gradually declining (**Fig. S1F**).

Collectively, our findings demonstrate that CHI3L1 is predominantly upregulated in astrocytes, with minimal co-localization with microglia, in the tMCAO mouse model of stroke. This spatiotemporal expression pattern underscores the importance of CHI3L1 in stroke pathophysiology and highlights its potential as a therapeutic target for future interventions.

2.2 CHI3L1 Overexpression and Knockdown in tMCAO Mice Uncovers Its Role in Stroke - Related Functional and Histological Changes

To investigate the role of CHI3L1 in stroke, we conducted a series of *in vivo* experiments. Lentiviral vectors were engineered to specifically modulate CHI3L1 expression (**Fig. 2A**). For overexpression, the full-length CHI3L1 cDNA was cloned into a lentiviral vector under the control of a strong promoter. For knockdown, short-hairpin RNAs (shRNAs) targeting CHI3L1 were inserted into a lentiviral backbone. Transfection of these constructs into 293T cells produced high-titer lentiviral particles.

We subsequently administered the CHI3L1-modulating lentiviruses into the cerebral cortex of tMCAO mice via multi-site injections. Western blot analysis validated the efficacy of CHI3L1 overexpression and knockdown in the brain tissues (**Fig. 2B**). Specific anti-CHI3L1 antibodies confirmed that lentiviral transduction successfully regulated CHI3L1 expression, establishing the feasibility of our experimental approach.

Motor function was assessed using the Garcia score, Neurological Deficit Score, rotarod test, and beam-walking test to evaluate neurological deficits and motor recovery post-stroke (**Fig. 2C–2E**). D0 denotes the time point before tMCAO (the final day of behavioral training), during which mice without tMCAO showed no statistically significant differences. CHI3L1 overexpression consistently impaired motor recovery, resulting in delayed coordination, more pronounced neurological deficits, and compromised fine motor control. In contrast, CHI3L1 knockdown significantly improved motor outcomes, with enhanced balance, fewer hindlimb slips, and faster task completion.

In the Open Field Test (OFT), designed to assess general locomotion and exploratory behavior, CHI3L1 overexpression restricted movement and exploration (**Fig. S3A- S3B**). Mice overexpressing CHI3L1 traveled shorter distances and made fewer entries into the center zone. In contrast, knockdown promoted locomotor activity and exploratory behavior. Cognitive performance, assessed by the Novel Object Location (NOL) Test and Novel Object Recognition (NOR) Test, revealed that CHI3L1 overexpression impaired spatial memory and object recognition abilities, as indicated by reduced exploratory preferences (**Fig. S3C–S3D**). Conversely, CHI3L1 knockdown enhanced cognitive function, reflected by increased preference for novel locations

and objects. Additionally, in sham-operated groups with viral manipulation but without tMCAO (**Fig. S3E–S3G**), no statistically significant differences were observed in open-field activity, novel location recognition, or novel object performance, confirming that the observed cognitive changes were specifically associated with CHI3L1 modulation rather than viral or surgical effects.

Physiological and histological analyses further substantiated these findings. Cerebral blood flow (CBF) measurements on day 7 post-tMCAO demonstrated that CHI3L1 overexpression was associated with reduced perfusion in the ischemic region, whereas knockdown improved CBF (**Fig. 2G**). Increased CBF reflects enhanced vascular remodeling, collateral formation, and functional perfusion recovery in the ischemic hemisphere. These improvements indicate better collateral circulation and vascular remodeling, supporting tissue viability and post-stroke recovery. TTC staining at 72 hours post-tMCAO revealed that CHI3L1 overexpression exacerbated infarct volume, indicating more severe tissue damage, while knockdown significantly reduced infarct size (**Fig. 2H**).

To assess neuronal apoptosis, we analyzed cleaved caspase-3 (Caspase3 p11) by Western blot in brain tissue from mice treated with CHI3L1-related lentiviruses after tMCAO (**Fig. S3H**). Consistent with previous results, CHI3L1 overexpression increased the levels of apoptosis-related proteins, whereas its knockdown reduced them, indicating that CHI3L1 promotes neuronal apoptosis following tMCAO.

Assessment of blood-brain barrier (BBB) integrity using the Evans blue assay showed that CHI3L1 overexpression increased BBB permeability, whereas knockdown preserved barrier function (**Fig. 2I**).

Immunohistochemical analysis of MAP2 and DAPI staining in the cerebral cortex and peri-infarct penumbra at 14 days post-stroke further elucidated the effects of CHI3L1 modulation (**Fig. 2J**). In the cortex, MAP2 fluorescence intensity showed no significant change following either CHI3L1 overexpression or knockdown. However, in the peri-infarct penumbra, CHI3L1 overexpression markedly reduced MAP2 intensity, indicating impaired neuronal repair, whereas its knockdown restored MAP2 levels, suggesting enhanced neuronal preservation and recovery.

Collectively, these findings highlight CHI3L1 as a pivotal modulator of stroke outcomes in the tMCAO model. The consistent pattern of worsened outcomes with CHI3L1 overexpression and improved outcomes with knockdown suggests that targeting CHI3L1 may represent a promising therapeutic approach to enhance functional recovery and mitigate brain damage following stroke.

2.3 Astrocyte - specific CHI3L1 Knockout in Chil1^{cKO} Mice: Impact on Stroke - related Behaviors, Physiology, and Neuronal Outcomes

To determine whether astrocyte-derived CHI3L1 contributes to stroke pathophysiology, we employed Chil1$^{flox/flox}$ and Chil1^{cKO} mice to achieve astrocyte-specific CHI3L1 knockout (**Fig. 3A**). Western blot analysis of brain tissue extracts, using specific anti-CHI3L1 antibodies, confirmed a significant reduction in CHI3L1 protein levels in Chil1^{cKO} mice compared to Chil1$^{flox/flox}$ controls (**Fig. 3B**), establishing the high efficiency of CHI3L1 ablation in the knockout model.

Motor function assessments revealed that, from day 3 to day 7 post- tMCAO, Chil1^{cKO} mice exhibited significantly improved recovery, as reflected by higher Garcia scores and lower Neurological Deficit Scores (**Fig. 3C**). In the rotarod test, Chil1^{cKO} mice displayed longer latencies to fall, indicating better motor coordination and balance (**Fig. 3D**). Beam-walking test results further supported superior performance in the Chil1^{cKO} group, with shorter platform-reaching times, fewer contralateral hindlimb slips, and lower Feeney scores, indicative of improved fine motor function (**Fig. 3E**).

In the OFT, Chil1^{cKO} mice traveled greater distances and entered the central area more frequently than Chil1$^{flox/flox}$ mice, suggesting enhanced locomotor activity and exploratory behavior (**Fig. S4A- S4B**).

Cognitive assessments using the NOL and (NOR tests demonstrated that Chil1^{cKO} mice exhibited higher exploratory preferences compared to controls, indicating improved spatial memory and object recognition capabilities (**Fig. S4C**).

Physiological and histological analyses corroborated these behavioral findings. On day 7 post-tMCAO, Chil1^{cKO} mice exhibited significantly better CBF in the ischemic hemisphere compared to controls (**Fig. 3F**). Infarct volume, assessed by 2,3,5-triphenyltetrazolium chloride (TTC) staining at 72 hours post-tMCAO, was markedly reduced in Chil1^{cKO} mice (**Fig. 3G**). Histological examination further demonstrated a lower number of lost neurons in the Chil1^{cKO} group (Fig. S4D). Blood-brain barrier (BBB) integrity, evaluated by Evans blue permeability assays at days 7 and 14 post-tMCAO, was better preserved in the Chil1^{cKO} group, as indicated by lower dye extravasation (**Fig. 3H**).

Immunohistochemical staining for MAP2 and DAPI in the peri-infarct penumbra at 14 days post-stroke revealed higher MAP2 fluorescence intensity in Chil1^{cKO} mice, suggesting improved neural recovery (**Fig. 3I**). To clarify the timing of CHI3L1-mediated neuronal death, we performed Western blot analysis of brain proteins from Chil1^{cKO} mice. Although CHI3L1 expression peaks between 3 and 7 days post-tMCAO, our results showed that cleaved caspase-3 levels were significantly lower in Chil1^{cKO} brains compared with Chil1$^{flox/flox}$ controls from day 1 to day 7 post-tMCAO. These findings indicate that CHI3L1 begins to mediate neuronal apoptosis as early as day 1 (and possibly earlier) after stroke, as reflected by the temporal dynamics of apoptotic protein activation (**Fig. S4C**).

To further determine the source of serum CHI3L1 elevation, we measured CHI3L1 levels in brain and serum samples from Chil1^{cKO} mice at day 3 post-tMCAO using ELISA. Brain CHI3L1 levels in Chil1^{cKO} mice were significantly lower than those in Chil1$^{flox/flox}$ mice. Although serum CHI3L1 levels were also reduced, they remained higher than those in sham-operated mice. These results suggest that astrocytes contribute to serum CHI3L1 after cerebral infarction, but not exclusively. Consistent with previous reports, serum CHI3L1 may also originate from other cell types, such as blood macrophages, inflammatory cells, or extra-cerebral glial cells. Given its association with disease progression, serum CHI3L1 is proposed as a potential clinical biomarker for cerebral infarction.

In summary, astrocyte-specific genetic ablation of CHI3L1 in Chil1^{cKO} mice significantly improved functional recovery after stroke, attenuated cerebral infarction,

preserved neurovascular integrity, and reduced neuronal apoptosis. These findings highlight CHI3L1 as a promising therapeutic target for ischemic stroke.

2.4 CHI3L1 - Neutralizing Antibody: Promoting Stroke Recovery and Holding Promise for Therapeutic Translation

We further evaluated the therapeutic potential of CHI3L1 inhibition by administering a CHI3L1-neutralizing antibody and comparing outcomes to a PBS-treated control group (**Fig. 3J**). Western blot analysis revealed significantly reduced CHI3L1 expression levels in the Anti-CHI3L1 group compared to PBS-treated mice. This confirmed the antibody's efficacy in lowering CHI3L1 expression following cerebral ischemia (**Fig. 3K**).

Motor function assessments demonstrated superior recovery in the Anti-CHI3L1 group. From day 0 to day 7 post-tMCAO, these mice exhibited higher Garcia scores and lower Neurological Deficit Scores relative to controls (**Fig. 3L**). In the rotarod test, Anti-CHI3L1-treated mice showed longer latencies to fall (**Fig. 3M**). Beam-walking tests revealed shorter platform-reaching times, fewer contralateral hindlimb slips, and lower Feeney scores, indicating enhanced fine motor skills (**Fig. 3N**). In the OFT, Anti-CHI3L1-treated mice traveled longer distances and made more center-area entries compared to the PBS group, suggesting improved locomotor activity and exploration (**Fig. S4G- S4H**). Cognitive assessments, including the NOL and NOR tests, demonstrated that Anti-CHI3L1 treatment enhanced spatial memory and object recognition. This was evidenced by increased exploratory preferences relative to the PBS group (**Fig. S4I**). Physiological and histological analyses supported these behavioral findings. On day 7 post-tMCAO, Anti-CHI3L1-treated mice exhibited improved CBF in the ischemic hemisphere compared to controls (**Fig. 3O**). TTC staining revealed a smaller infarct volume in the Anti-CHI3L1 group, indicating reduced brain tissue damage (**Fig. 3P**). The Evans blue permeability assay showed lower BBB permeability in Anti-CHI3L1-treated mice, reflecting better preservation of barrier integrity (**Fig. 3Q**). Immunohistochemical analysis of MAP2 and DAPI staining in the peri-infarct penumbra at 14 days post-stroke revealed higher MAP2 fluorescence intensity in the Anti-CHI3L1 group, suggesting enhanced neuronal preservation and recovery (**Fig. 3R**). The promising outcomes observed with CHI3L1 neutralization support the therapeutic potential of this approach. Administering a CHI3L1-neutralizing antibody shortly after stroke onset may minimize brain damage, enhance functional recovery, and offer a novel treatment strategy for acute ischemic stroke.

Additionally, we evaluated the long-term therapeutic potential of CHI3L1 neutralization by administering a CHI3L1-neutralizing antibody to mice after tMCAO and monitoring outcomes over an extended period (**Fig. S5A**). This assessment included long-term motor function, cognitive performance, cerebral blood flow, and neuronal preservation, all of which showed sustained improvements in the Anti-CHI3L1 group (**Fig. S5**). These findings confirm that post-stroke CHI3L1 inhibition is an effective therapeutic approach and demonstrate that such intervention enhances long-term - recovery, further supporting the potential of CHI3L1-targeted strategies for clinical translation in ischemic stroke treatment.

In conclusion, astrocyte-specific CHI3L1 knockout in Chil1^{cKO} mice demonstrated that astrocyte-derived CHI3L1 contributes significantly to stroke pathophysiology, and antibody-mediated neutralization further improved stroke-related outcomes. Together, these findings underscore the potential of targeting CHI3L1 through genetic or pharmacological means as a promising therapeutic approach for ischemic stroke.

2.5 Astrocytic CHI3L1 activates NLRP3 signaling via GAL3, influencing neuronal apoptosis and suggesting GAL3 as a stroke - treatment target

Primary astrocytes were transfected with CHI3L1-modulating lentiviruses (Lenti-NC, Lenti-CHI3L1, Lenti-shCHI3L1-1, Lenti-shCHI3L1-2) for 48 hours. Following transfection, cells were subjected to 6 hours of oxygen-glucose deprivation followed by 24 hours of reoxygenation (OGD6h-Re24h) (**Fig. S6A**). TUNEL staining revealed that neither CHI3L1 overexpression nor knockdown influenced astrocyte apoptosis during OGD injury. This suggests that CHI3L1 does not directly regulate astrocyte survival under these conditions (**Fig. S6B**). To investigate the impact of astrocyte-derived CHI3L1 on neuronal outcomes, we collected astrocyte-conditioned medium (ACM) from transfected astrocytes exposed to OGD and applied it to primary cortical neurons undergoing OGD-Re (**Fig. 4A**). Western blot analysis of cleaved caspase-3 in neurons showed that CHI3L1 overexpression in astrocytes increased neuronal apoptosis, whereas CHI3L1 knockdown reduced it (**Fig. 4B**). Morphological analyses revealed alterations in dendritic complexity consistent with these apoptotic changes (**Fig. 4C**). TUNEL staining further confirmed that neurons treated with ACM from CHI3L1-overexpressing astrocytes exhibited more apoptosis. In contrast, ACM from CHI3L1-knockdown astrocytes conferred protection (**Fig. 4D**). Importantly, no significant differences in neuronal apoptosis were observed under non-OGD conditions (**Fig. S6C–S6D**), indicating that astrocytic CHI3L1 primarily influences neuronal survival under ischemic stress. To investigate the role of CHI3L1 in blood–brain barrier (BBB) regulation in vitro, we established a Transwell co-culture system of astrocytes and mouse brain microvascular endothelial cells (bEnd.3) (**Fig. S6E**). When CHI3L1-overexpressing astrocytes were co-cultured with endothelial cells under OGD conditions, BBB integrity was compromised, as indicated by reduced transendothelial electrical resistance (TEER) (**Fig. S6F**) and increased sodium fluorescein (NaF) permeability (**Fig. S6G**). Conversely, CHI3L1 knockdown in astrocytes alleviated OGD-induced BBB disruption. These findings demonstrate that CHI3L1 promotes BBB breakdown under ischemic conditions *in vitro*.

To elucidate downstream signaling mechanisms, primary cortical astrocytes were treated with recombinant CHI3L1 protein (250 ng/mL) and analyzed by RNA sequencing. Principal component analysis (PCA) demonstrated distinct gene expression profiles between CHI3L1-treated and PBS-treated astrocytes. Differential expression analysis highlighted significant changes, including upregulation of NLRP3 (**Fig. S7A–S7C**). KEGG pathway enrichment analysis revealed significant activation of the NOD-like receptor signaling pathway. This implicated NLRP3 signaling as a downstream target of CHI3L1 (**Fig. 4E**). Immunofluorescence staining further confirmed that NLRP3 expression in astrocytes (GFAP$^+$) was significantly increased in the

peri-infarct region of tMCAO mice compared with the contralateral side. This finding is consistent with the transcriptional data and supports astrocytic NLRP3 as a downstream mediator of CHI3L1 signaling in ischemic stroke (**Fig. 4F**).

To identify the receptor mediating CHI3L1 signaling, we first utilized lentiviral constructs targeting six candidate receptors (TMEM219, RAGE, GAL3, CD44, CRTH2, IL13Rα2) to knock down their expression in primary astrocytes. Following CHI3L1 treatment and OGD exposure, Western blot analysis showed that knockdown of GAL3, but not other candidates, abrogated CHI3L1-induced activation of NLRP3, Caspase-1, pre-IL-1β, and IL-1β (**Fig. 4G–4H**).

We then performed immunofluorescence staining in the peri-infarct region of tMCAO mice to examine these six candidate receptors. Among them, only GAL3 exhibited increased expression in astrocytes within the peri-infarct region, where CHI3L1 is highly expressed. Co-staining for GAL3 and GFAP confirmed ipsilateral upregulation of GAL3 relative to the contralateral hemisphere (**Fig. S7D, 4I–4J**). Partial co-localization of GAL3 with microglia was also observed; however, quantitative analysis of $GAL3^+GFAP^+$ and $GAL3^+IBA1^+$ cells in the peri-infarct region indicated that GAL3 is predominantly associated with astrocytes (**Fig. 4K**). These findings suggest that astrocyte-derived GAL3 in the peri-infarct region may serve as the primary receptor mediating CHI3L1-induced activation of the NLRP3 inflammasome under ischemic conditions. To validate these findings *in vivo*, we stereotactically injected mice with CHI3L1 protein alone, CHI3L1 protein combined with Lenti-shGAL3, or Lenti-shGAL3 alone, followed by tMCAO induction. On day 5 post-stroke, proteins from ipsilateral and contralateral hemispheres were collected for Western blot analysis (**Fig. 4L**). Results indicated that co-treatment with Lenti-shGAL3 notably inhibited NLRP3 pathway activation compared to the CHI3L1-protein-only group, suggesting that GAL3 knockdown may effectively block CHI3L1-mediated NLRP3 activation in vivo (**Fig. 4M**).

To further clarify the downstream functional consequences of the CHI3L1–NLRP3 axis, we investigated its role in neuronal injury through the CHI3L1–NLRP3–IL-1β pathway. First, we confirmed that OGD-Re stimulation of primary astrocytes significantly increased the secretion of CHI3L1 and its downstream effector IL-1β in the conditioned medium (**Fig. S7E**). To verify that IL-1β contributes to neuronal damage, primary neurons were treated with recombinant IL-1β (10 ng/ml). Sholl analysis revealed marked morphological alterations (**Fig. S7G**), and TUNEL staining demonstrated a significant increase in neuronal apoptosis (**Fig. S7H**), identifying IL-1β as a key mediator of neuronal injury.

To exclude direct effects of CHI3L1 on neurons, astrocyte-derived conditioned medium (post-OGD-Re) was pretreated with either a CHI3L1-neutralizing antibody or an IL-1β-neutralizing antibody before being applied to neurons subjected to OGD-Re. Sholl analysis and apoptosis assays showed that only pretreatment with the IL-1β-neutralizing antibody significantly mitigated OGD-Re-induced neuronal injury, whereas CHI3L1 neutralization had no detectable protective effect (**Fig. S7I–S7K**).

Collectively, these findings demonstrate that astrocyte-derived CHI3L1 activates NLRP3 to promote IL-1β release, and that IL-1β directly induces neuronal damage—thereby establishing the functional importance of the CHI3L1–NLRP3–IL-1β axis in ischemic stroke pathology.

Collectively, these observations suggest that astrocyte-derived CHI3L1 in the peri-infarct region may act as a potential activator of the NLRP3 inflammasome via the GAL3 receptor, with IL-1β serving as a key downstream mediator of neuronal injury. This raises the possibility that targeting GAL3 could represent a promising therapeutic approach for ischemic stroke, though further investigation is needed to confirm its clinical relevance.

2.6 Blocking GAL3 Signaling Pathway in Astrocytes Using AAV - Mediated Knockdown: A Novel Strategy for Stroke Treatment

To investigate the role of astrocytic GAL3 in mediating CHI3L1-related effects on neurons, we utilized astrocyte-conditioned medium (ACM). Primary astrocytes were transfected with either Lenti-NC or Lenti-shGAL3 and subjected to oxygen-glucose deprivation followed by reoxygenation (OGD-Re). The resulting ACM was applied to primary cortical neurons undergoing OGD-Re (**Fig. S8A**). Neurons treated with ACM derived from CHI3L1-protein/OGD-Re-stimulated astrocytes exhibited pronounced morphological alterations, which were attenuated by ACM from shGAL3-transfected astrocytes (**Fig. S8B**). TUNEL staining further demonstrated that neurons exposed to ACM from CHI3L1-stimulated astrocytes displayed increased apoptosis, whereas ACM from shGAL3-transfected astrocytes mitigated this effect (**Fig. S8C**). Western blot analysis confirmed efficient GAL3 knockdown in astrocytes and revealed corresponding alterations in cleaved caspase-3 levels in neurons, reflecting changes in apoptotic signaling based on the source of ACM (**Fig. S8D**). To investigate the role of astrocyte-derived CHI3L1/GAL3 in regulating BBB integrity under ischemic conditions in vitro, we found that CHI3L1 overexpression in astrocytes reduced TEER and increased NaF permeability, indicating BBB impairment. In contrast, GAL3 knockdown, or combined CHI3L1 overexpression with GAL3 knockdown, restored TEER and decreased NaF permeability. Collectively, these results demonstrate that astrocyte-derived CHI3L1 disrupts BBB integrity through GAL3 under ischemic conditions, highlighting GAL3 as a potential therapeutic target for preserving BBB function in ischemic stroke (**Fig. S8E–S8F**). Given the central role of stroke as a major health burden, we next investigated the therapeutic potential of blocking GAL3 signaling using adeno-associated virus (AAV)-mediated gene knockdown (**Fig. 5A**). Following stereotaxic injection of cAAV constructs into the mouse cortex, GFP, GFAP, and DAPI staining confirmed specific targeting of astrocytes (**Fig. 5B**). Western blotting validated the effectiveness of AAV-shGAL3 in significantly reducing GAL3 expression in the ischemic brain compared to AAV-NC controls (**Fig. S8G**).

Motor function recovery was assessed using Garcia scores, Neurological Deficit Scores, rotarod, and beam-walking tests. Statistical analysis demonstrated that GAL3 knockdown significantly improved motor performance across all assessments, indicating enhanced functional recovery post-stroke (**Fig. 5C–5E**). Behavioral evaluations,

including the OFT, NOL Test, and NOR Test, further confirmed improved performance in AAV-shGAL3-treated mice compared to controls. This supported a positive effect of GAL3 inhibition on post-stroke cognitive and exploratory behaviors (**Fig. 5F–5G**). Histological and physiological analyses provided corroborative evidence. TTC staining demonstrated a reduction in infarct volume following GAL3 knockdown (**Fig. 5H**). CBF measurements showed improved perfusion in the ischemic hemisphere (**Fig. 5I**), while the Evans blue assay indicated decreased blood-brain barrier (BBB) permeability (**Fig. 5J**), collectively highlighting the neurovascular benefits of GAL3 blockade. Immunohistochemical staining of MAP2 in the peri-infarct penumbra revealed that GAL3 knockdown promoted neuronal preservation and recovery, as indicated by a higher density of MAP2-positive neurons compared with the control group (**Fig. 5K**).In parallel, Western blot analysis revealed that, when compared to AAV - NC, AAV - shGAL3 treatment effectively reduced both the levels of cleaved caspase - 3 and the expression of proteins associated with the NLRP3 signaling pathway, suggesting an attenuation of neuronal apoptosis (**Fig. 5L**). To further confirm that astrocyte-derived GAL3 in the peri-infarct region mediates the downstream effects of CHI3L1, we administered recombinant CHI3L1 protein together with astrocyte-specific AAV-shGAL3 or AAV-NC in mice, followed by tMCAO induction. The results showed that GAL3 knockdown in astrocytes effectively attenuated CHI3L1-induced infarct expansion (TTC staining) (**Fig. S8H**), reduced BBB disruption (Evans Blue assay) (**Fig. S8I**), and promoted neuronal preservation and recovery in the peri-infarct penumbra (MAP2 immunofluorescence) (**Fig. S8J**). Collectively, these findings demonstrate that astrocyte-derived GAL3 mediates the detrimental effects of CHI3L1 on infarct size, BBB integrity, and neuronal survival after ischemic stroke, further establishing GAL3 as a critical therapeutic target.

2.7 A GAL3 - Targeting Small - Molecule Inhibitor GB1107 Shows Promise in Stroke Treatment by Improving Multiple Pathophysiological Aspects

Stroke remains a leading cause of death and disability worldwide, underscoring the urgent need for innovative therapeutic strategies. In this study, we evaluated the potential repurpose of GB1107, a GAL3-targeting small-molecule inhibitor originally developed for oncology applications, as a treatment for ischemic stroke. To assess the influence of GB1107 on neuronal outcomes, we collected astrocyte-conditioned medium (ACM) from astrocytes treated with varying concentrations of GB1107 (1 μM, 10 μM, 50 μM). Following GB1107 treatment, astrocytes were subjected to oxygen-glucose deprivation followed by reoxygenation (OGD-Re). The resulting ACM was then applied to primary cortical neurons also undergoing OGD-Re (**Fig. 6A**). Neuronal morphology was analyzed by MAP2 staining. In the absence of exogenous CHI3L1 protein, GB1107 at 1 μM significantly improved neuronal morphology (**Fig. 6B**). When CHI3L1 protein was present, a higher concentration of GB1107 (10–50 μM) was required to achieve noticeable improvements in dendritic structure, as demonstrated by distinct morphological differences across treatment groups. Apoptosis was assessed by TUNEL staining. In the absence of CHI3L1 protein, GB1107 at 1 μM reduced neuronal apoptosis. In the presence of CHI3L1, the anti-apoptotic effect of

GB1107 was only observed within the 10–50 μM concentration range (**Fig. S9A**). These findings were further corroborated by Western blot analysis, which confirmed the concentration-dependent inhibition of cleaved caspase-3 expression by GB1107 under both conditions (**Fig. 6C**).

Together, these *in vitro* results indicate that GB1107 modulates neuronal morphology and reduces apoptosis via astrocyte-mediated signaling, with its efficacy modulated by CHI3L1 levels. To investigate the *in vivo* effects of GB1107, mice subjected to tMCAO were treated with intraperitoneal injections of GB1107 every other day. In a subset of mice, lentiviral overexpression of CHI3L1 was performed to further probe the interaction between CHI3L1 signaling and GB1107 treatment (**Fig. 6D**).

Motor function was evaluated using Garcia scores, Neurological Deficit Scores, rotarod, and beam-walking tests. Statistical analyses demonstrated that GB1107 treatment significantly improved motor recovery at multiple time points post-stroke (**Fig. 6E–6G**). Behavioral assessments revealed further benefits. In the OFT, GB1107-treated mice traveled greater distances and made more center crossings compared to controls (Fig. S9B). Similarly, in the NOL and NOR tests, GB1107 treatment enhanced exploratory behavior, indicating improved cognitive function following stroke (**Fig. S9C**).

Histological analyses confirmed the neuroprotective effects of GB1107. TTC staining demonstrated a significant reduction in infarct volume in GB1107-treated mice (**Fig. S9D**). CBF measurements on day 7 post-tMCAO revealed that GB1107 improved CBF in the ischemic hemisphere (**Fig. S9E**). Immunohistochemical staining of MAP2 in the peri-infarct penumbra revealed that GB1107 promoted neuronal preservation and recovery, as evidenced by a reduced loss of MAP2-positive neurons compared with vehicle-treated controls (**Fig. 6H**).

Furthermore, Western blot analysis revealed that intraperitoneal injection of GB1107 could reduce the levels of cleaved caspase - 3 and the expression of proteins associated with the NLRP3 signaling pathway (**Fig. S9F**). To evaluate the therapeutic potential of GB1107, we analyzed its pharmacokinetics in tMCAO mice following administration, measuring drug concentrations in serum, contralateral, and ipsilateral brain tissue at multiple time points (**Fig. S9G**), along with plasma-to-brain concentration ratios (**Fig. S9H**). These results provide essential pharmacokinetic evidence supporting the potential clinical translation of GB1107.

Collectively, the findings support GB1107 as a promising therapeutic candidate for the treatment of ischemic stroke.

3 Figures

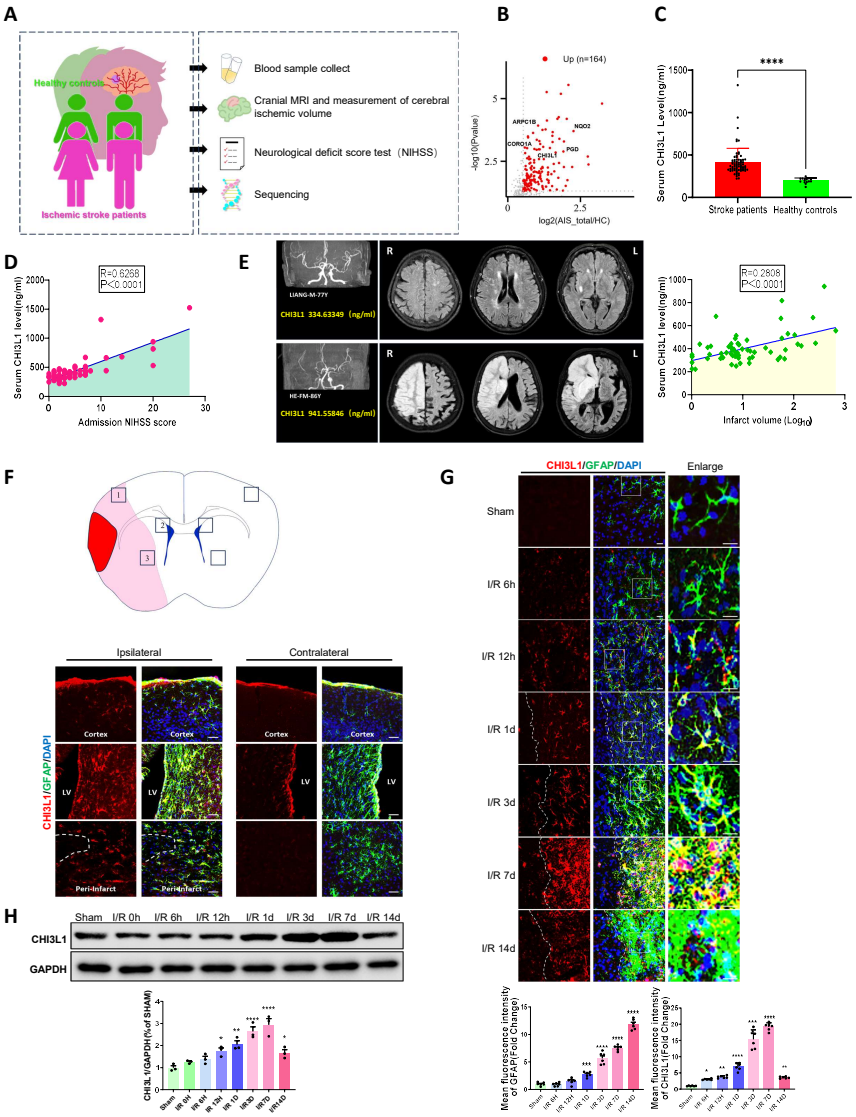

Fig. 1 Profiling of CHI3L1 in Acute Ischemic Stroke Patients and tMCAO Mouse Models
(A) Schematic diagram illustrating the collection of clinical data, serum samples, imaging information, NIHSS scores, and processing for proteomic sequencing.
(B) High-throughput protein expression analysis using Data-Independent Acquisition (DIA) sequencing of acute ischemic stroke (AIS) patients ($n = 24$) and healthy controls (HC, $n = 11$).
(C) Serum CHI3L1 levels measured by ELISA in AIS patients ($n = 70$) and HC ($n = 15$). Statistical significance assessed by Student's t-test. Data are presented as mean ± SD.
(D-E) Correlations between serum CHI3L1 levels and admission NIHSS scores (D, $n = 70$) and ischemic brain volume (E, $n = 62$).
(F-G) Immunohistochemical staining of GFAP (green) and CHI3L1 (red) in various brain regions and at different time points after tMCAO; nuclei counterstained with Hoechst (blue). White dotted lines mark infarction border zones (IBZs). Scale bars = 20 μm ($n = 6$ mice).
(H) Western blot analysis of CHI3L1 expression in ischemic hemispheres at different time points post-tMCAO ($n = 5$ per group).
Statistical significance: $**p < 0.01$; $***p < 0.001$; $****p < 0.0001$. Data are presented as mean ± SEM.

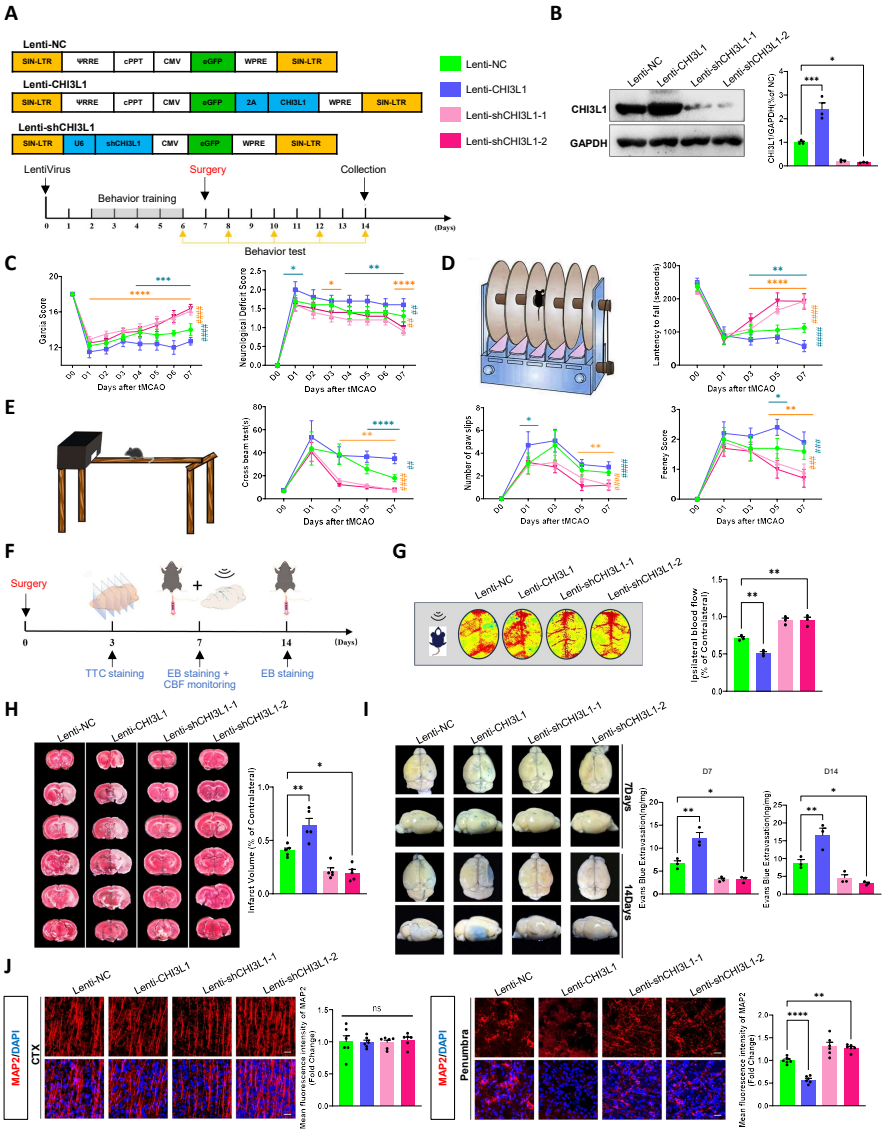

Fig. 2 Functional Impact of Lentivirus-Mediated CHI3L1 Manipulation in a Mouse Model of Ischemic Stroke

(A) Schematic of four lentiviral constructs targeting CHI3L1 (Lent-NC, overexpression, Lenti-shCHI3L1-1, Lenti-shCHI3L1-2).

(B) Western blot validation of CHI3L1 overexpression and knockdown efficiency (n = 3 per group).

(C–E) Motor function recovery assessed by Garcia scores, Neurological deficit scores (C), rotarod test (D), and beam-walking test (E) over 7 days post-tMCAO (n = 10 mice per group). Orange bars signify comparisons between the NC group and the CHI3L1 knockdown group, while blue bars indicate comparisons between the NC group and the CHI3L1 overexpression group. Significance levels: $*p < 0.05$; $**p < 0.01$; $***p < 0.001$; $****p < 0.0001$ compared to the NC group at indicated time points; $\#p < 0.05$; $\#\#p < 0.01$; $\#\#\#p < 0.001$; $\#\#\#\#p < 0.0001$ compared to the NC group throughout the entire experiment.

(F) Timeline of experimental procedures.

(G) Cerebral blood flow (CBF) assessment by laser speckle imaging (n = 3 per group).

(H) Infarct volume quantified by TTC staining at 72 h post-tMCAO (n = 3 per group).

(I) Blood-brain barrier (BBB) permeability evaluated by Evans blue assay at days 7 and 14 post-tMCAO (n = 3 mice per group).

(J) Immunohistochemistry of MAP2 (red) and DAPI (blue) in cortex and peri-infarct penumbra at 14 days post-stroke (n = 6).

Data analyzed by one-way ANOVA or two-way ANOVA (for repeated measures). Significance thresholds: $*p < 0.05$; $**p < 0.01$; $***p < 0.001$; $****p < 0.0001$. Data are presented as mean ± SEM.

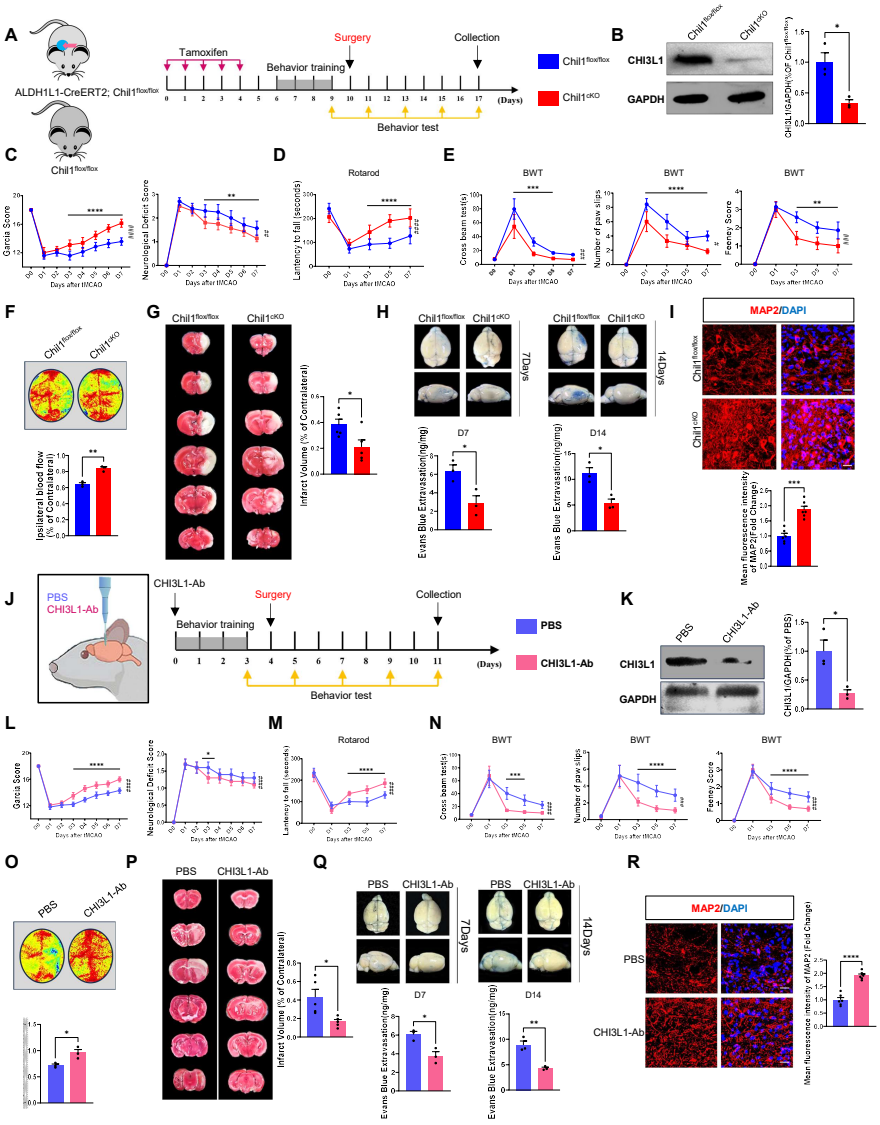

Fig. 3 Genetic and Pharmacological Manipulation of CHI3L1 in Mouse Ischemic Stroke Models
(A) Schematic of experimental timeline for knockout mice and anti-CHI3L1 antibody interventions.
(B) Western blot validation of CHI3L1 knockdown in Chil1cKO mice (n = 3).
(C–E) Motor behavior assessments (Garcia scores, Neurological deficit scores, rotarod, beam-walking) 7 days post-tMCAO (n = 7 mice per group). Significance levels: $*p < 0.05$; $**p < 0.01$; $***p < 0.001$; $****p < 0.0001$ compared to the control mice at indicated time points; $\#p < 0.05$; $\#\#p < 0.01$; $\#\#\#p < 0.001$; $\#\#\#\#p < 0.0001$ compared to the control mice across the entire experiment.
(F–I) Physiological evaluations: CBF, infarct volume (TTC staining), BBB permeability (Evans blue assay), and MAP2 immunostaining in Chil1cKO and control mice.
(J) Timeline for anti-CHI3L1 antibody experiments.
(K) Western blot validation of CHI3L1 knockdown after antibody injection (n = 3).
(L–N) Behavioral tests (n = 10 per group) for PBS versus anti-CHI3L1-treated mice. $*p < 0.05$; $**p < 0.01$; $***p < 0.001$; $****p < 0.0001$ compared to the PBS group at indicated time points; $\#p < 0.05$; $\#\#p < 0.01$; $\#\#\#p < 0.001$; $\#\#\#\#p < 0.0001$ compared to the PBS group across the entire experiment.
(O–R) Physiological outcomes: CBF, infarct volume, BBB permeability, and MAP2 staining.
Statistical significance assessed by two-way ANOVA, Student's t-test, or Mann–Whitney test, as appropriate. Significance thresholds: $*p < 0.05$; $**p < 0.01$; $***p < 0.001$; $****p < 0.0001$. Data are presented as mean ± SEM.

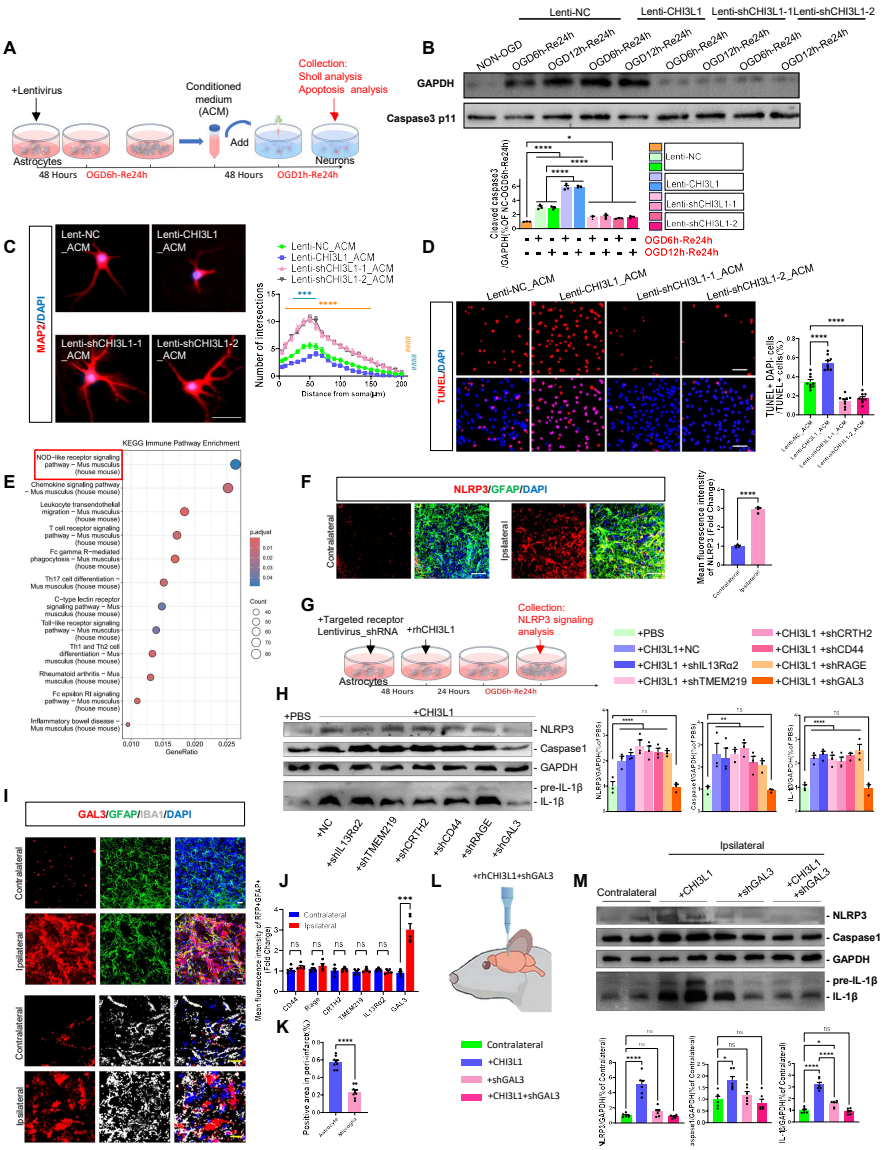

Fig. 4 Cellular and Molecular Mechanisms of CHI3L1 in Modulating the NLRP3 Signaling Pathway
(A) Schematic of in vitro experiment: astrocyte transfection, ACM collection, and neuronal OGD/Re treatment.
(B) Neuronal apoptosis measured by cleaved caspase-3 expression (n = 3 biological replicates).
(C) sholl analysis of neuronal dendritic complexity (n = 15 neurons from 3 independent experiments). Orange bars represent comparisons between the Lenti-NC ACM group and CHI3L1 knockdown ACM groups (Lenti-shCHI3L1-1 ACM and Lenti-shCHI3L1-2 ACM); blue bars represent comparisons between the Lent-NC ACM group and CHI3L1 overexpression group (Lenti-CHI3L1 ACM). Significance levels: $*p < 0.05$; $**p < 0.01$; $***p < 0.001$; $****p < 0.0001$ compared to the Lent-NC ACM group at indicated distance; $\#p < 0.05$; $\#\#p < 0.01$; $\#\#\#p < 0.001$; $\#\#\#\#p < 0.0001$ compared to the Lent-NC ACM group across the entire distance.
(D) Quantification of TUNEL-positive neurons treated with different ACM preparations (n = 9 from 3 independent experiments).
(E) KEGG pathway enrichment from RNA-seq of CHI3L1-treated astrocytes (n = 4 per group).
(F) Immunofluorescence of NLRP3 (red) and GFAP (green) in ipsilateral and contralateral hemispheres post-tMCAO.
(G–H) Knockdown of six candidate receptors and assessment of NLRP3 pathway activation by Western blot (n = 3 per group).
(I-K) Immunofluorescence of GAL3 (red), GFAP (green), IBA1(silver) in ipsilateral and contralateral hemispheres post-tMCAO.
(L–M) In vivo validation: stereotaxic injection of CHI3L1-protein ± Lenti-shGAL3, and analysis of NLRP3 pathway activation by Western blot (n = 6).
Statistical significance evaluated using one-way ANOVA or Kruskal–Wallis test. Significance thresholds: $*p < 0.05$; $**p < 0.01$; $***p < 0.001$; $****p < 0.0001$. Data are presented as mean ± SEM.

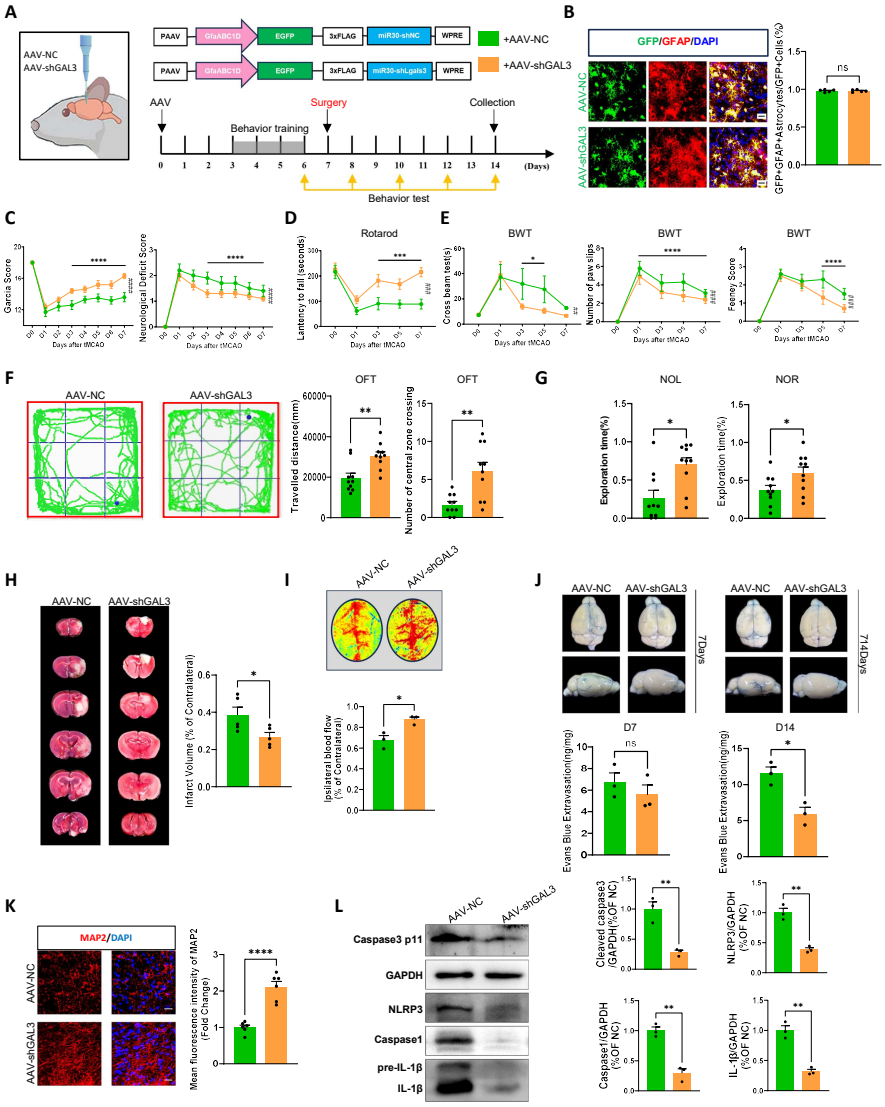

Fig. 5 Role of GAL3 in Mouse Ischemic Stroke Models Using AAV-Mediated Gene Silencing in Astrocytes

(A) Schematic of stereotaxic AAV injection, tMCAO modeling, and behavioral testing timeline.

(B) Immunofluorescence confirmation of AAV-GFP expression in astrocytes (GFP+, GFAP+).

(C–E) Motor function recovery assessments (Garcia scores, Neurological deficit scores, rotarod, beam-walking) (n = 10 per group). Significance levels: $*p < 0.05$; $**p < 0.01$; $***p < 0.001$; $****p < 0.0001$ compared to the AAV-NC group at indicated time points; $\#p < 0.05$; $\#\#p < 0.01$; $\#\#\#p < 0.001$; $\#\#\#\#p < 0.0001$ compared to the AAV-NC group across the entire experiment.

(F–G) Behavioral tests: Open field test (OFT), Novel object location (NOL) test, and Novel object recognition (NOR) test (n = 10 per group).

(H–J) Physiological measurements: infarct volume (TTC staining, n = 5), CBF (n = 3), and BBB permeability (n = 3).

(K) MAP2 immunostaining in peri-infarct penumbra at 14 days post-stroke (n = 6).

(L) Western blot analysis of cleaved caspase-3 levels and assessment of NLRP3 pathway (n = 3).

Data analyzed by one-way ANOVA or two-way ANOVA with repeated measures. Significance thresholds: $*p < 0.05$; $**p < 0.01$; $***p < 0.001$; $****p < 0.0001$. Data are presented as mean ± SEM.

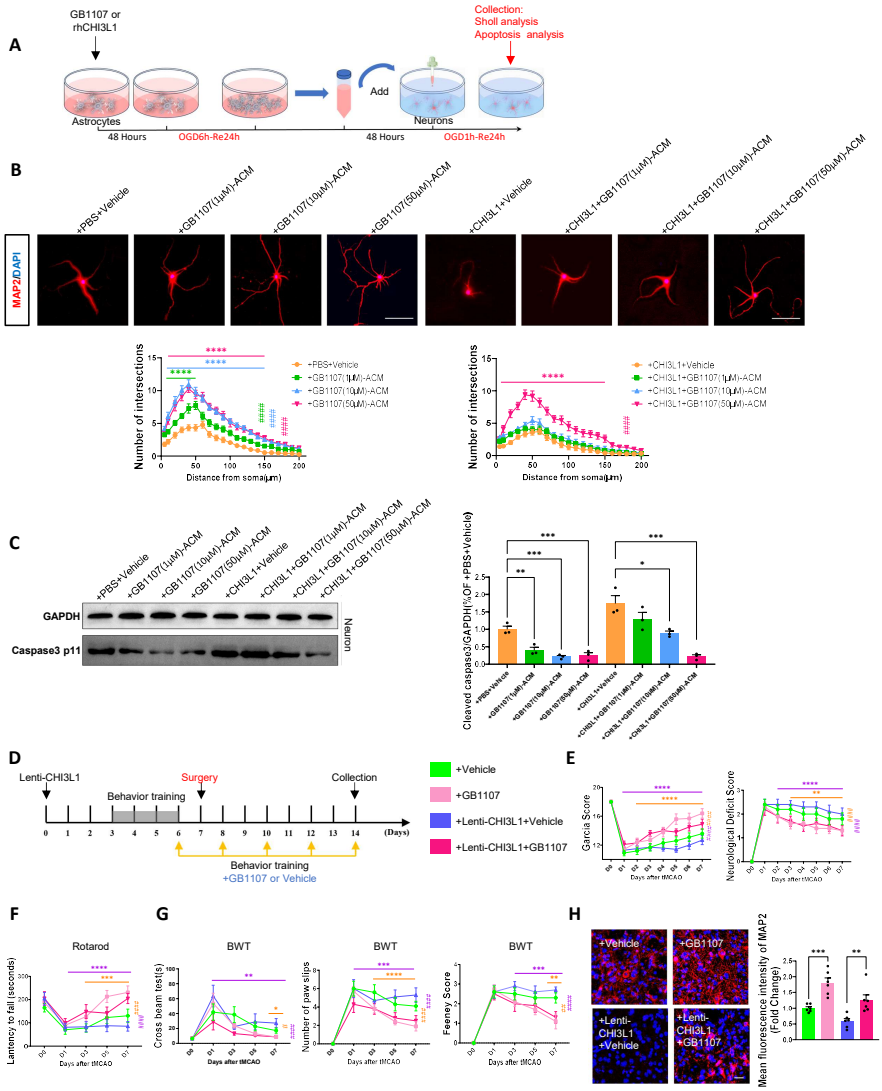

Fig. 6 Therapeutic Intervention Using GB1107 in CHI3L1-Mediated Stroke Models
(A) Primary astrocytes were divided into multiple groups. Some groups were treated with different concentrations of GB1107 (0 μM, 1 μM, 10 μM, 50 μM), while other groups were treated with both rhCHI3L1 and different concentrations of GB1107. After 48 hours of treatment, all astrocytes were subjected to oxygen - glucose deprivation for 6 hours followed by reoxygenation for 24 hours (OGD6h - Re24h). The conditioned medium (ACM) from these astrocytes was then collected. Primary - cultured neurons were treated with the respective ACMs for 48 hours and subsequently subjected to oxygen - glucose deprivation for 1 hour and reoxygenation for 24 hours (OGD1h - Re24h). Finally, Sholl analysis and apoptosis analysis were conducted on the neurons.
(B) Neuronal Morphology Analysis was performed on neurons treated with ACM from astrocytes exposed to different treatments. Representative images of MAP2 (red) and DAPI (blue) staining are shown. Green bars represent comparisons between the 0 μM and 1 μM groups; blue bars represent comparisons between the 0 μM and 10 μM groups; red bars represent comparisons between the 0 μM and 50 μM groups. N = 15 neurons from 3 independent experiments. Scale bar = 10 μm. Significance levels: $*p < 0.05$; $**p < 0.01$; $***p < 0.001$; $****p < 0.0001$ compared to the 0 μM group at indicated distances; $\#p < 0.05$; $\#\#p < 0.01$; $\#\#\#p < 0.001$; $\#\#\#\#p < 0.0001$ compared to the 0 μM group across the entire distance.
(C) Western blotting was used to quantify cleaved caspase-3 (Caspase3 p11) levels in neurons treated with ACM from the various astrocyte conditions. n = 3 per group. GAPDH or β-actin served as loading controls.
(D) Schematic of study design with stereotaxic lentiviral injection, GB1107 systemic administration, and behavioral testing.
(E–G) Motor behavior assessments (Garcia scores, Neurological deficit scores, rotarod, beam-walking) in four experimental groups (n = 10 per group). Orange bars compare the Vehicle and GB1107 groups; purple bars compare the Lenti-CHI3L1+Vehicle and Lenti-CHI3L1-GB1107 groups. Significance levels: $*p < 0.05$; $**p < 0.01$; $***p < 0.001$; $****p < 0.0001$ for differences at specific time points; $\#p < 0.05$; $\#\#p < 0.01$; $\#\#\#p < 0.001$; $\#\#\#\#p < 0.0001$ for differences across the entire experiment.
(H) MAP2 immunostaining in peri-infarct penumbra at 14 days post-stroke (n = 6).
Statistical significance assessed by one-way ANOVA, two-way ANOVA, or Kruskal–Wallis test as appropriate. Significance levels: $*p < 0.05$; $**p < 0.01$; $***p < 0.001$; $****p < 0.0001$. Data are presented as mean ± SEM.

4 Methods

4.1 Animals and Genotyping

Wild-type C57BL/6 male mice (6–8 weeks old) were obtained from Vital River Laboratories and maintained under standardized conditions at the Guangdong Laboratory Animals Monitoring Institute, with ad libitum access to food and water. Chil1 conditional knockout (cKO) mice were generated by crossing $Chil1^{flox/flox}$ ($Chil1^{f/f}$) mice with tamoxifen-inducible ALDH1L1-CreER mice. $Chil1^{f/f}$ littermates were used as controls. Genotyping was performed to confirm the generation of $Chil1^{cKO}$ mice; the primer sequences used for genotyping are listed in Table S4. Tamoxifen (HY-13757A, MedChem Express) was dissolved in corn oil at a concentration of 30 mg/mL and administered by intraperitoneal injection at a dose of 180 mg/kg for five consecutive days to induce Cre-mediated recombination. All animal experiments were conducted in accordance with protocols approved by the Institutional Animal Care and Use Committee of Sun Yat-sen University.

4.2 Murine Models of Acute Cerebral Ischemic Stroke Induced by tMCAO/R

Murine models of focal acute ischemic stroke were established tMCAO to simulate ischemia/reperfusion injury. Mice were anesthetized with 1.5–2.0% isoflurane, and body temperature was maintained at 37 ± 0.5°C using a heating pad throughout the procedure. A silicone-coated monofilament was introduced into the right internal carotid artery via the right common carotid artery and advanced to occlude the origin of the right middle cerebral artery (MCA) for 60 minutes. After the occlusion period, the filament was carefully withdrawn to initiate reperfusion. Mice exhibiting less than 70% reduction in CBF during occlusion or less than 70% recovery within 10 minutes of reperfusion, as well as mice with intraoperative brain hemorrhage or mortality, were excluded from further analyses. Sham-operated mice underwent the same surgical procedures without filament insertion. Following surgery, mice were placed in a temperature-controlled incubator for 4 hours before being returned to their home cages. All experimental procedures were conducted in accordance with ethical guidelines to minimize animal suffering. The overall surgical mortality rate was recorded at 13.38%.

4.3 Neurological Deficit and Garcia scoring

Neurological deficits were assessed daily for seven days following ischemia-reperfusion injury. A neurological deficit score ranging from 0 to 4 was used, where 0 indicated no apparent deficit, 1 represented weakness in the ipsilateral forelimb, 2 denoted circling toward the ipsilateral side, 3 indicated body imbalance and trunk inclination toward the ipsilateral side, and 4 reflected no spontaneous motor activity or death. Sensorimotor functions were evaluated using the Modified Garcia Score at 1–7 days after tMCAO. Assessments were performed by an observer blinded to the experimental groups. The Modified Garcia Score comprised six subtests, each scored from 0 to 3, with higher scores indicating milder injury. The maximum total score was 18 points.

The evaluated parameters included: (1) spontaneous activity, (2) symmetry of forelimb movement, (3) forepaw extension, (4) climbing ability, (5) body proprioception, and (6) response to vibrissae touch.

4.4 Human Serum Sample Collection and CHI3L1 Level Measurement

This prospective cohort study consecutively enrolled 77 patients with first-ever acute ischemic stroke (AIS), confirmed by brain computed tomography (CT) or magnetic resonance imaging (MRI), at The Third Affiliated Hospital of Sun Yat-sen University between January 2023 and December 2024. Inclusion criteria were: (1) age > 18 years and (2) hospitalization within 24 hours of symptom onset. Exclusion criteria included recurrent stroke, arthritis, infection, autoimmune disease, malignancy, severe hepatic or respiratory disease, pregnancy, or hormone therapy. To enable stroke subtype analysis, the enrollment criteria explicitly excluded patients with recent atrial fibrillation, valvular heart disease, or other cardiogenic risk factors. As a result, the enrolled AIS cohort primarily comprised patients with the large-artery atherosclerotic subtype. Age-matched healthy controls without cerebrovascular disease were recruited from the hospital's health examination center during the same period. The study was approved by the Ethics Committee of The Third Affiliated Hospital of Sun Yat-sen University.

Written informed consent was obtained from all participants or their legal representatives. Demographic data, vascular risk factors (e.g., smoking, alcohol consumption, hypertension, diabetes mellitus, and other relevant medical histories), time from symptom onset, and stroke severity assessed by the National Institutes of Health Stroke Scale (NIHSS) at admission and discharge were recorded for all participants. In addition, magnetic resonance imaging (MRI) including magnetic resonance angiography (MRA) was performed. Ischemic lesion volume was calculated using the modified formula:

$$Volume = \frac{A \times B \times C \times 0.5}{2 \text{ ml}} \tag{1}$$

where A and B represent the maximum perpendicular diameters of the largest infarct cross-section on FLAIR images, and C is the number of slices with a thickness of 5 mm. Detailed patient and control information is provided in Table S3. For CHI3L1 level measurement, heparin-anticoagulated blood samples were centrifuged at 3000 rpm for 15 minutes at 4°C, and the serum supernatant was collected. Human CHI3L1 concentrations were quantified using a commercial ELISA kit (MEIMIAN, MM-1816H1), and absorbance was measured at 450 nm.

4.5 Primary Cerebral Cortical Neuron and Astrocyte Culture and Oxygen-Glucose Deprivation/Reoxygenation (OGD/Re) Model

Primary cortical neurons and astrocytes were isolated from the cerebral cortices of 1-day-old C57BL/6 mouse neonates. Brain tissues were digested with 0.25% trypsin

at 37°C for 10 minutes, and enzymatic activity was terminated by the addition of complete culture medium. After removal of the medium, tissues were resuspended in 10 mL of complete culture medium, treated with DNase solution for 5 minutes at room temperature, and gently washed twice with complete medium. The resulting cell suspension was filtered through a sterile 40 μm nylon cell strainer. For neuronal cultures, cells were maintained in neurobasal medium (Gibco, 21103-049) supplemented with 2% B-27 (Gibco, 17504-044), 0.5 mM L-glutamine (Sigma-Aldrich, G8540), and 100 U/mL penicillin/streptomycin (Beyotime Biotechnology, C0222). For astrocyte cultures, cells were maintained in DMEM/F12 medium (Gibco, 11330) containing 10% fetal bovine serum (Gibco, 10099) and 100 U/mL penicillin/streptomycin (Beyotime Biotechnology, C0222). Both neuronal and astrocytic cultures were incubated at 37°C in a humidified atmosphere containing 5% CO_2. Cell purity was assessed by immunocytochemistry using the neuronal marker MAP2 for neurons and the astrocytic marker GFAP for astrocytes; in both cases, purity exceeded 95%. To establish the oxygen-glucose deprivation (OGD) model, culture medium was replaced with glucose-free DMEM (Gibco, #11966), and cells were placed in a sealed hypoxia chamber (Billups-Rothenberg, CA, USA) filled with a gas mixture of 95% N_2 and 5% CO_2 for the designated duration. For reoxygenation (Re), cells were returned to a normoxic incubator, and the medium was replaced with complete glucose-containing medium. Control cells were maintained under normoxic conditions in standard glucose-containing DMEM. For the preparation of astrocyte-conditioned medium (ACM), primary astrocytes were subjected to OGD for 6 hours followed by 24 hours of reoxygenation. ACM was collected, filtered through a 0.22 μm nylon mesh (BS-QT-037, Biosharp), and supplemented with additional factors before use as a culture medium for primary neurons.

4.6 Lentivirus and Retrovirus Packaging and Cell Transfection

Lentivirus and retrovirus packaging were performed as previously described. Briefly, HEK293T cells at 70-90% confluency were co-transfected with retroviral or lentiviral transfer vector DNA along with helper packaging plasmids (CMV-GP and VSVG for retrovirus; psPAX2 and pMD2.G for lentivirus) using polyethyleneimine (PEI; PR40001, Proteintech Group). Four hours after transfection, the medium was replaced with complete DMEM supplemented with 10% fetal bovine serum (FBS) and 1% penicillin-streptomycin. Viral particles were harvested from the culture medium at 48, 72, and 96 hours post-transfection, filtered through a 0.22 μm filter (Biosharp, BS-QT-037), and concentrated by ultracentrifugation (Beckman Coulter SW32 Ti rotor) at 20,000 rpm for 2 hours at 4°C. Concentrated viral stocks achieved titers of 10^8–10^9 TU/mL and were resuspended in 100 μL of complete medium, then stored at -80°C until use. For cell transfection, second-passage primary astrocytes or primary cortical neurons were transduced following standard protocols. Astrocytes were seeded at 2×10^5 cells per well, and 1 hour prior to transfection, the culture medium was replaced with neuron culture medium lacking penicillin-streptomycin. Lentiviruses (1×10^8 TU/mL, 5-20 μL) were diluted in enhanced infection solution and added to the cells. After 72 hours, the medium was replaced with fresh astrocyte culture medium supplemented with either PBS (control) or recombinant CHI3L1 protein (500 ng/mL).

Transfection efficiency was validated by Western blot analysis. Transfected cells were subsequently used for immunofluorescence staining or protein extraction.

4.7 Establishment of an In Vitro Blood-Brain Barrier Model

An *in vitro* blood–brain barrier (BBB) model was established using a Transwell co-culture system with three experimental groups: (1) Blank group (cell-free inserts), (2) Co-culture NON-OGD group, and (3) Co-culture OGD group. Astrocytes were seeded on the basolateral side of the Transwell inserts at a density of 1×10^7 cells/mL (200 μL suspension) and incubated for 6 hours. The inserts were then inverted and transferred to a 24-well plate. Mouse brain microvascular endothelial cells (bEnd.3) were seeded into the apical chamber at 1×10^5 cells/mL (600 μL), while the basolateral chamber was filled with 1.2 mL of astrocyte-specific culture medium. The co-culture system was maintained for 5 days before subsequent assays.

4.8 Measurement of Transendothelial Electrical Resistance

Transepithelial electrical resistance (TEER) was measured using an epithelial voltammeter. Standard electrodes were calibrated to 1000 Ω before each use. The measuring electrodes were sterilized in 75% ethanol for 30 minutes and equilibrated in phosphate-buffered saline (PBS) for 15 minutes. After stabilization, TEER values were recorded using short apical and long basolateral electrodes. The final TEER value was calculated as follows: TEER ($\Omega \cdot \mathrm{cm}^2$) = (Measured TEER value - Blank TEER value) $\times$ membrane surface area.

4.9 Assessment of Paracellular Permeability

Paracellular permeability was assessed by measuring the flux of sodium fluorescein (NaF) across the endothelial–astrocyte barrier. After OGD or control treatment, 300 μL of NaF solution (10 μg/mL) was added to the apical chamber, while the basolateral chamber was filled with 800 μL of PBS. Following a 1-hour incubation at 37°C, 100 μL of the basolateral medium was collected for analysis. Fluorescence intensity was measured at excitation and emission wavelengths of 485 nm and 535 nm, respectively. NaF concentration was calculated from a standard curve, and the corresponding permeability coefficient was derived accordingly.

4.10 Stereotaxic Injection of Viruses and CHI3L1 Antibody

For *in vivo* viral delivery, mice were anesthetized with isoflurane and securely positioned in a stereotaxic apparatus (RWD Life Science, Shenzhen, China). A midline scalp incision was made, and a small burr hole (approximately 1 mm in diameter) was drilled into the skull at predetermined coordinates relative to the bregma. Using a 26-gauge needle connected to a 10 μL gas-tight glass syringe (Hamilton), 1 μL of viral suspension ($titer > 1 \times 10^9$ viral particles/mL) or 50 μg of CHI3L1 antibody was injected into the target cortical region. The injection was performed at a rate of 0.1 μL/min. Following injection, the needle was left in place for 10 minutes to minimize reflux, then slowly withdrawn over an additional 5 minutes. Mice were allowed

to recover in a temperature-controlled chamber and were monitored until resumption of normal activity. The nucleotide sequences of the viral constructs used are listed in Table S4. Eight-week-old C57BL/6J mice received a single microinjection of either the viral preparation or CHI3L1 antibody into the ipsilateral cortex at the ischemic lesion site. The injection coordinates relative to the bregma were as follows: 0.3 mm anterior, 3 mm lateral, and 2 mm deep (AP: 0.3, ML: 3, depth: 2); 1.9 mm posterior, 3 mm lateral, and 2 mm deep (AP: –1.9, ML: 3, depth: 2).

4.11 Drug Treatment

GB1107 (HY-114409, MedChem Express) was dissolved in dimethyl sulfoxide (DMSO) to prepare a stock solution at a concentration of 50 mg/mL, which was stored at –80°C until use. For *in vitro* experiments, the stock solution was diluted with complete culture medium to achieve final concentrations of 1 μM, 10 μM, and 50 μM. GB1107 was administered to primary astrocytes on the first day after the initial passage. For *in vivo* experiments, GB1107 was diluted in corn oil to a final dosage of 15 mg/kg per mouse and administered by intraperitoneal injection. Treatment commenced one day prior to surgery and continued with injections administered every 48 hours thereafter.

4.12 Pharmacokinetic Analysis

Plasma and brain tissue concentrations of GB1107 were quantified by liquid chromatography-tandem mass spectrometry (LC-MS/MS). For plasma samples, a 50 μL aliquot was protein-precipitated with 300 μL of ice-cold methanol containing 1 ng/mL regorafenib (internal standard). After vortexing (10 min) and centrifugation (15,000 rpm, 10 min, 4°C), the supernatant was analyzed. Brain tissue ($\tilde{0}$.2 g) was homogenized in 80% methanol, and a 50 μL aliquot of the homogenate was processed identically to the plasma protocol. Samples exceeding the calibration range were appropriately diluted with blank matrix prior to re-analysis.

4.13 Infarct Volume Measurement (2,3,5-triphenyltetrazolium chloride (TTC) staining)

Mice were euthanized 72 hours after ischemia-reperfusion (I/R) injury. Infarct volume was assessed using 2,3,5-triphenyltetrazolium chloride (TTC) staining (Solarbio, T8170).

Briefly, brains were harvested and coronally sectioned into 2 mm thick slices using a brain mold. The slices were incubated in 2% TTC solution prepared in phosphate buffer (PB) at room temperature. TTC-stained viable brain tissue appeared red, while infarcted regions remained pale.

The infarct area was calculated as the difference between the TTC-stained (red) area of the contralateral hemisphere and the ipsilateral hemisphere for each slice. Brain atrophy volume was quantified using ImageJ software. The ratio of brain atrophy was calculated according to the following formula: Brain atrophy (%) = (Sum of the ischemic (white) areas across all slices) / (Sum of the total brain slice areas) $\times$ 100%.

4.14 Blood-Brain Barrier Permeability Assay

Blood-brain barrier (BBB) integrity was assessed 7 or 14 days after ischemia-reperfusion (I/R) injury. Mice were intravenously injected via the tail vein with 2% Evans blue (EB; 4 mg/kg; Sigma-Aldrich, E2129) dissolved in sterile phosphate-buffered saline (PBS). Four hours post-injection, mice were sacrificed, and brains were harvested and weighed. Evans blue was extracted by homogenizing brain tissue and incubating it in formamide at 55°C for 24 hours. The absorbance of the supernatant was measured at 620 nm, and EB concentrations were determined using a standard curve. Results were normalized to those from sham-operated mice and expressed as nanograms of Evans blue per milligram of brain tissue.

4.15 Cerebral Blood Flow Imaging

Cerebral blood flow (CBF) was measured using the PeriCam PSI System, a laser speckle contrast analysis (LASCA)-based perfusion imaging device. This system provides real-time images of cortical blood flow based on changes in laser speckle patterns. During imaging, mice were anesthetized with 1.25% isoflurane in oxygen and maintained at 37°C using a heated pad. Post-stroke imaging was performed on day 7 after tMCAO, with each session lasting less than 10 minutes. Results were expressed as the percentage of CBF in the ischemic hemisphere relative to the contralateral hemisphere.

4.16 Western Blot Analysis

Tissue samples and cultured cells were homogenized and lysed in ice-cold radioimmunoprecipitation assay (RIPA) buffer (P0013, Beyotime) supplemented with protease inhibitors (P1006, Beyotime) and phosphatase inhibitors (P1045, Beyotime) for 30 minutes. Lysates were centrifuged at 12,000 rpm for 15 minutes at 4°C to isolate total protein. Protein concentrations were quantified using a BCA Protein Assay Kit (P0012S, Beyotime). The samples were mixed with 5× loading buffer (P0015, Beyotime), boiled at 96°C for 10 minutes, separated by SDS-PAGE, and transferred to polyvinylidene difluoride (PVDF) membranes. Membranes were blocked with 5% skim milk in TBST for 1 hour at room temperature, incubated overnight at 4°C with primary antibodies, and then with horseradish peroxidase (HRP)-conjugated secondary antibodies for 1–2 hours at room temperature. Protein bands were visualized using enhanced chemiluminescence (ECL) reagents and imaged with a Tanon 5500 Imaging System. Quantitative analysis was performed using ImageJ software. Primary antibodies included Mouse anti-GAPDH (1:1000, Beyotime, # AF0006), Mouse anti-βactin (1:1000, Huabio, # M1210-2), Rabbit anti-CHI3L1 (1:1000, Solarbio, Cat# K109584P), Rabbit anti-Gal3 (1:1000, Proteintech, # 14979-1-AP), Mouse anti-Cleaved-caspase3(1:1000, CST, Cat# 9661S), Rabbit anti-NLRP3 (1:1000, Beyotime, Cat# AF2155), Mouse anti-Caspase1 (1:1000, Santa Cruz Biotechnology, Cat# sc-392736), Mouse anti-IL-1β (1:1000, Santa Cruz Biotechnology, Cat# sc-52012).

4.17 Immunofluorescence Staining and Analysis

Mice were deeply anesthetized with 2% pentobarbital sodium and transcardially perfused with PBS followed by 4% paraformaldehyde (PFA). Brains were post-fixed overnight in 4% PFA, cryoprotected in 30% sucrose at 4°C, and coronally sectioned at 30 μm thickness using a freezing microtome. Sections were stored in cryoprotectant solution at 4°C until staining. For immunofluorescence staining, sections were blocked with 3% goat serum and 0.25% Triton X-100 in PBS for 1 hour at room temperature and incubated with primary antibodies overnight at 4°C. After PBS washes, sections were incubated with fluorophore-conjugated secondary antibodies for 1 hour at room temperature in the dark. Nuclei were counterstained with DAPI (Sigma-Aldrich, #2261b), and sections were mounted with polyvinyl alcohol (PVA; Polysciences, #02815). Imaging was performed using a Leica TCS SP8 confocal microscope with excitation wavelengths of 405, 488, 568, and 647 nm. Quantitative evaluation of fluorescence intensity was performed using ImageJ software. At least three randomly selected fields per section and three biological replicates per group were analyzed, with all experiments independently repeated at least three times. Primary antibodies included Rabbit anti-CHI3L1 (1:500, Solarbio, Cat# K109584P), Rabbit anti-Gal3 (1:500, Proteintech, # 14979-1-AP), Mouse anti-GFAP (1:1000, CST, # 3670S), Rabbit anti-GFAP (1:1000, CST, # 12389S), Mouse anti-IBA1 (1:500, Servicebio, # GB12105), Rabbit anti-MAP2 (1:500, Proteintech, # 17490-1-AP), Rabbit anti-NeuN (1:500, Abcam, # 177487), Rabbit anti-IL13Rα2 (1:200, Biorbyt, # orb114178), Mouse anti-TMEM219 (1:200, Abmart, # M030834), Mouse anti-CRTH2 (1:200, Santa Cruz Biotechnology, # sc-271898) , Rabbit anti-CD44 (1:200, Proteintech, # 15675-1-AP), Rabbit anti-Rage (1:200, Proteintech, # 16346-1-AP).

4.18 Neuronal Morphology Analysis Using the Sholl Method

Neuronal morphology, including the number and length of neuritic processes, was assessed using Sholl analysis in Fiji-ImageJ. Morphological analyses were performed on neurons subjected to oxygen-glucose deprivation and reoxygenation (OGD/Re). For each experimental condition, at least 15 neurons derived from three independent cultures were analyzed to ensure statistical robustness.

4.19 TUNEL Staining for Apoptosis Detection

Apoptosis was detected using the TUNEL BrightRed Apoptosis Detection Kit (Vazyme,# A113-03) according to the manufacturer's instructions. Quantification of TUNEL-positive and DAPI-positive cells was performed in at least three sections from three independent animals per group.

4.20 Behavioral Tests

4.20.1 Rotarod Test

Motor coordination and balance were assessed using an accelerating rotarod apparatus. Prior to middle cerebral artery occlusion (tMCAO), mice were trained for three consecutive days to acclimate to the task. Testing was conducted on days 1, 3, 5, and

7 post-stroke. During testing, mice were required to balance and walk on a rotating cylinder, with the speed increasing from 10 rotations per minute (rpm) to 40 rpm over a 2.5-minute period. Each mouse underwent three trials with 30-minute intervals between trials. The time each mouse remained on the rotarod was recorded, and the average performance was calculated.

4.20.2 Beam-Walking Test

The beam-walking test evaluated fine motor coordination. A cylindrical ridged wooden beam (10 mm in diameter, 100 cm in length) was positioned 70 cm above the bench top. The experiment included a 3-day training phase prior to tMCAO, during which mice were trained to traverse the beam into a dark box. Each mouse received three training sessions per day. During testing, the time taken for each mouse to traverse the beam was recorded, with a maximum allowed time of 2 minutes. The number of paw slips was documented. Additionally, the Feeney score was used to assess motor deficits according to the following criteria: 0 = traverses the beam without falling; 1 = traverses the beam with $< 50\%$ probability of falling; 2 = traverses the beam with $> 50\%$ probability of falling; 3 = traverses the beam but the paralyzed hindlimb does not assist forward movement; 4 = unable to traverse the beam but can sit on it; 5 = falls immediately after being placed on the beam

4.20.3 Open Field Test (OFT)

The open field test (OFT) was used to evaluate anxiety-like behaviors and general locomotor activity. The testing apparatus consisted of a square arena (50 cm $\times$ 50 cm $\times$ 50 cm) with transparent walls, under bright lighting conditions. The floor was virtually divided into peripheral and central zones. Prior to testing, mice were acclimated to the experimental room to minimize stress. Each mouse was placed in the center of the arena and allowed to explore freely for 10 minutes. Movements were recorded with an automated tracking system (Panlab system and SMART v3.0 software), and key parameters, including total distance traveled and time spent in the central zone, were analyzed. The arena was thoroughly cleaned with 70% ethanol between trials to eliminate olfactory cues.

4.20.4 Novel Object Location Test(NOL)

The novel object location (NOL) test assessed spatial memory and cognitive function. Testing was conducted in a square open field arena (50 cm diameter) and consisted of three phases: habituation, training, and testing. Habituation phase (Day 1): Mice explored the empty arena for 10 minutes. Training phase (Days 2 and 3): Two identical objects (object A on day 2, object B on day 3) were placed in opposite corners, and mice explored for 10 minutes each day. Testing phase (Day 4): Two identical objects (object B) were placed in parallel locations, with one object moved to a novel position. Mice were allowed to explore for 10 minutes. The novel location preference score was calculated novel location preference score = $\frac{\text{Time spent exploring the object in the novel location}}{\text{Total time spent exploring both objects}} \times 100\%$

The arena and objects were cleaned with 75% ethanol after each session. Behavioral analyses were performed by blinded observers based on recorded video footage.

4.20.5 Novel Object Recognition Test(NOR)

The novel object recognition (NOR) test evaluated recognition memory. Testing was performed in three phases: Adaptation phase: Mice explored an empty arena (50 cm $\times$ 50 cm $\times$ 50 cm) for 10 minutes. Training phase (Days 1 and 2): Mice explored two identical objects (object A on day 1, object B on day 2) placed in parallel locations for 10 minutes each day. Testing phase (Day 3): One familiar object (object B) was replaced with a novel object (object C), and mice were allowed to explore for 10 minutes.

The discrimination index was calculated as:

discrimination index= $\frac{\text{Time spent exploring the novel object C}}{\text{Total time spent exploring objects B and C}} \times 100\%$

The arena and objects were sanitized with 75% ethanol between sessions to prevent olfactory bias. Behavioral data were recorded and analyzed using video-based tracking by blinded observers.

4.21 Statistical analysis

Statistical analyses were performed using GraphPad Prism version 9, and all graphs were generated using the same software. Data are presented as mean $\pm$ standard error of the mean (SEM). For comparisons between two groups, either an unpaired two-tailed Student's t-test or a Mann–Whitney test was used, depending on the distribution of the data. Comparisons among multiple groups were analyzed using one-way or two-way analysis of variance (ANOVA), followed by Tukey's multiple comparisons test or Kruskal–Wallis test, as appropriate. For specific datasets involving repeated measures, such as neurological deficit scores, repeated measures ANOVA was used with false discovery rate (FDR) correction, employing the two-stage linear step-up procedure of Benjamini, Krieger, and Yekutieli. The normality of data distribution was assessed using the Shapiro–Wilk test. A p-value of < 0.05 was considered indicative of a non-normal distribution. Statistical significance was set as follows: $p* < 0.05$; $p** < 0.01$; $p*** < 0.001$; $p**** < 0.0001$. Sample sizes were not predetermined by statistical methods due to the lack of available effect size estimates prior to experimentation. Sample sizes for each experimental group are provided in the corresponding figure legends. No pre-established exclusion criteria were applied. Descriptive statistics were used to analyze demographic and neuropsychological data. Relationships between CHI3L1 levels and both NIHSS scores and ischemic brain volume were evaluated using Pearson correlation analysis. All experiments included at least three independent biological replicates.

5 Discussion

5.1 CHI3L1 as a Key Player in Stroke Pathophysiology

This study provides comprehensive insights into the role of CHI3L1 in stroke. Initial proteomic analysis of acute ischemic stroke (AIS) patients not only replicated previous findings of elevated CHI3L1 levels but also identified a suite of co-dysregulated proteins and key signaling pathways, including NLRP3, MAPK, PI3K-Akt, and TNF signaling[27, 34, 35]. The observed positive correlations between CHI3L1 levels, stroke severity (NIHSS scores), and infarct volume strongly support its significance in stroke pathophysiology. These findings position CHI3L1 as a potential biomarker for early diagnosis and prognosis in stroke patients[27, 33].

Notably, prior work by Im et al. (2020)1 explored CHI3L1 in stroke, suggesting that CHI3L1 deletion may exacerbate stroke via enhanced neuroinflammation and it is proposed that CHI3L1 may regulate stroke outcomes through microglial polarization. In the context of this prior exploration, our study provides new insights into CHI3L1's cellular localization and functional context in stroke. Using immunofluorescence co-localization, primary cell models, and public single-cell sequencing data (GEO, Fig. S2), we observed that CHI3L1 upregulation in the tMCAO model occurs predominantly in astrocytes ($GFAP^+$), with minimal co-localization in microglia ($IBA1^+$). This finding refines the current understanding by indicating that CHI3L1 likely exerts its effects primarily through astrocyte–neuron interactions and astrocyte-mediated inflammatory processes, offering a more detailed perspective on CHI3L1's role in stroke pathophysiology.

In the tMCAO mouse model and *in vitro* OGD model, CHI3L1 was predominantly upregulated in astrocytes. This is supported by immunofluorescence data showing co-localization of CHI3L1 with GFAP-positive astrocytes in peri-infarct regions. The dynamic increase in CHI3L1 expression following stroke-like insults aligns with emerging concepts that highlight the significance of glial-neuronal interactions in stroke outcomes. Astrocytes are known to release various factors that influence neuronal survival, inflammation, and tissue repair following stroke[36, 37]. Upregulation of CHI3L1 may represent part of a complex astrocyte-mediated response that modulates these processes. The temporal dynamics of CHI3L1 expression in astrocytes following ischemic insult are particularly notable. In the tMCAO model, CHI3L1 levels increased in the peri-infarct zone as early as 24 hours and remained elevated through day 7, suggesting an active and sustained role in the glial response to injury. Given the established function of reactive astrocytes in regulating extracellular glutamate, maintaining barrier integrity, and modulating neuroinflammation[35, 37–40], CHI3L1 may act as a context-dependent regulator that amplifies neurotoxic signaling under ischemic conditions.

A key aspect of our study is the rationale for selecting CHI3L1 as a therapeutic target, particularly since our proteomic screen (Fig. 1B) identified several other proteins with marked acute alterations. We focused on CHI3L1 based on three converging lines of evidence. First, multiple clinical studies have established serum CHI3L1 as a reliable prognostic biomarker for stroke, a foundation that many other altered proteins lack. Second, our ELISA data from supplementary cohorts demonstrated a dose-dependent

relationship between CHI3L1 levels and stroke severity indicators such as NIHSS scores and infarct volume, linking it directly to stroke progression rather than to general tissue injury. Third, CHI3L1 represents an inflammation-associated molecule with known neurological relevance but incomplete characterization in cerebral infarction, positioning it as a mechanistically significant bridge between neuroinflammation and ischemic injury.

Other proteins identified in the proteomic analysis-such as CORO1A and PGD (related to neuronal morphogenesis), S100A12 and ARPC1B (involved in inflammation), and ADH1A/ADH1B and NQO2 (associated with metabolism)—also warrant attention. Although their specific roles in stroke remain unexplored, their potential involvement highlights additional molecular pathways worth investigating in future studies to expand our understanding of stroke pathophysiology.

5.2 Functional Consequences of CHI3L1 Manipulation

Specifically, CHI3L1 overexpression led to increased infarct volumes and worsened neurological scores, while knockdown reduced infarct size and improved behavioral outcomes. Overexpression impaired cognitive and motor functions, increased infarct volume, reduced cerebral blood flow, compromised blood-brain barrier (BBB) integrity, and decreased neuronal preservation. Conversely, CHI3L1 knockdown significantly improved functional outcomes and reduced tissue damage[7]. These findings highlight the potential of targeting CHI3L1 as a therapeutic strategy for stroke. Our conditioned medium experiments underscore the importance of astrocyte-neuron crosstalk in stroke pathology. Neurons exposed to media from CHI3L1-overexpressing astrocytes exhibited increased apoptosis and simplified dendritic architecture, even in the absence of direct ischemic insult. This indicates that astrocytic CHI3L1 is sufficient to propagate neurotoxic signals, potentially through the secretion of pro-inflammatory mediators or EVs. These findings emphasize the role of astrocytes not merely as passive responders, but as active drivers of secondary neuronal injury. In support of this, Sholl analysis of dendritic complexity revealed that ACM from CHI3L1-overexpressing astrocytes significantly reduced neurite arborization, while knockdown preserved structural integrity. These data add morphological evidence to the pro-apoptotic influence of astrocyte-derived CHI3L1 and reinforce the importance of astrocyte-to-neuron signaling in ischemia. Astrocyte-specific knockout of CHI3L1 in $\text{Chil1}^{\text{cKO}}$ mice further confirmed the detrimental role of astrocyte-derived CHI3L1. Improved behavioral, physiological, and histological outcomes in $\text{Chil1}^{\text{cKO}}$ mice after stroke provide *in vivo* genetic evidence supporting the pathogenic contribution of CHI3L1. Similarly, administration of a CHI3L1-neutralizing antibody promoted stroke recovery, reinforcing the therapeutic potential of CHI3L1 inhibition [8]. Across multiple experimental conditions, MAP2 staining consistently revealed greater preservation of neuronal structures in the treatment and knockdown groups, further substantiating the neuroprotective effects of CHI3L1 inhibition and its downstream signaling blockade. These results are particularly significant given the current lack of effective therapies for stroke. However, further studies are necessary to optimize the delivery, dosage, and timing of CHI3L1-targeted therapies.

5.3 CHI3L1 Signaling Pathway and GAL3 as a Therapeutic Target

We identified GAL3 as the downstream receptor through which CHI3L1 activates the NLRP3 signaling pathway. *In vitro* experiments with primary astrocytes and *in vivo* validation consistently showed that CHI3L1 activation of NLRP3 signaling was mediated via GAL3, leading to neuronal apoptosis[9, 25]. This discovery of the CHI3L1–GAL3–NLRP3 axis provides a novel molecular mechanism underlying ischemic neuronal injury.

Targeting GAL3 emerges as a promising therapeutic strategy. Both AAV-mediated knockdown of GAL3 in astrocytes and pharmacological inhibition with the small-molecule inhibitor GB1107 led to significant improvements across multiple outcome measures. These included motor and cognitive performance, infarct volume, cerebral blood flow, BBB integrity, and neuronal preservation[41–43]. These findings suggest that inhibition of GAL3 signaling could be an effective approach to mitigate stroke-induced damage. Notably, the in vivo knockdown of GAL3 in astrocytes not only reduced NLRP3 pathway activation but also led to consistent improvements across multiple functional domains. These included motor coordination, memory, and anxiety-like behavior. These behavioral improvements were accompanied by smaller infarct volumes, restored cerebral blood flow, and preservation of $MAP2^{+}$ neurons. This convergence of molecular, histological, and behavioral data strongly supports the candidacy of GAL3 as a central mediator of CHI3L1's deleterious effects and a viable pharmacological target. Importantly, our receptor screen revealed that among six potential CHI3L1-interacting receptors, only GAL3 was consistently upregulated in ischemic astrocytes. This selectivity underscores GAL3's unique role in mediating downstream NLRP3 activation. It also sets GAL3 apart from other candidates like CD44 or RAGE, which did not alter NLRP3 signaling upon knockdown.

Small-molecule inhibitors like GB1107 are particularly attractive due to their drug-like properties; however, further optimization of their pharmacokinetic and pharmacodynamic profiles is necessary. GB1107's efficacy in reducing infarct size and improving neurological outcomes in the tMCAO model underscores its potential as a therapeutic agent targeting GAL3. Potential off-target effects must also be carefully assessed, given the physiological functions of GAL3 beyond the brain[43–46]. Notably, CHI3L1 knockout, antibody neutralization, and GAL3 inhibition all yielded consistent neuroprotective effects, suggesting a robust and targetable signaling axis. These findings not only validate the CHI3L1–GAL3–NLRP3 pathway as a pathogenic mechanism but also provide multiple entry points for therapeutic development.

A key unresolved question concerns the upstream regulation of CHI3L1 - specifically, why its upregulation occurs selectively in astrocytes following ischemia. We hypothesize that this specificity results from the combined influence of Stat3 pathway activation, the ischemia-induced inflammatory microenvironment, and intrinsic astrocyte epigenetic properties. Previous studies have demonstrated Stat3 activation after ischemic stroke, and in non-stroke disease models, such as tumor systems, Stat3 acts as an upstream regulator of CHI3L1. Moreover, p-Stat3-positive reactive astrocytes have been reported to secrete CHI3L1. Future work will aim to elucidate the

Stat3–CHI3L1 axis in cerebral infarction models to clarify the molecular mechanisms driving astrocyte-specific CHI3L1 upregulation after ischemia.

5.4 Clinical Implications and Future Directions

The findings of this study have several important clinical implications. CHI3L1 could serve as a biomarker for stroke, aiding early diagnosis, prognosis evaluation, and patient stratification. Furthermore, therapeutic strategies targeting CHI3L1 or its downstream effector GAL3, through neutralizing antibodies or small-molecule inhibitors like GB1107, represent promising avenues for clinical translation[47, 48]. *In vitro*, GB1107 demonstrated a dose-dependent ability to mitigate CHI3L1-induced neuronal stress, as evidenced by reduced apoptosis and preserved neurite morphology. This effect was modulated by the presence of exogenous CHI3L1, suggesting a direct pharmacodynamic interaction with astrocyte-derived signaling.

5.5 Limitations of the Study

Several limitations should be acknowledged. First, *in vitro* models such as the OGD model simplify the complex *in vivo* brain environment and lack critical components such as the full immune system and vascular network, which may influence ischemic responses[49, 50]. Additionally, the OGD model does not account for the dynamic interactions between neurons, glia, and endothelial cells present in vivo, potentially limiting the translatability of findings. Second, the tMCAO mouse model, although widely used, has intrinsic limitations, including species-specific differences in brain anatomy and stroke pathology, which may affect translatability to humans[51, 52]. Third, our proteomic analysis was conducted on a relatively small AIS patient cohort ($n = 16$), necessitating validation in larger, more diverse populations to confirm CHI3L1's biomarker potential and associations with clinical subtypes. Finally, while this study focused on the CHI3L1–GAL3–NLRP3 axis, it is possible that other parallel or compensatory signaling pathways contribute to stroke pathophysiology and warrant further investigation[53–55].

In conclusion, this study clarifies the critical role of CHI3L1 and its downstream effector GAL3 in the pathophysiology of stroke and provides preclinical evidence supporting GAL3 signaling as a viable therapeutic target. Collectively, our findings not only elucidate the CHI3L1–GAL3–NLRP3 axis in stroke pathology but also identify actionable targets for therapeutic intervention, paving the way for novel treatment strategies in ischemic stroke.

6 Conclusion

This study clarifies the critical role of CHI3L1 and its downstream effector GAL3 in the pathophysiology of stroke and provides preclinical evidence supporting GAL3 signaling as a viable therapeutic target. Collectively, our findings not only elucidate the CHI3L1–GAL3–NLRP3 axis in stroke pathology but also identify actionable targets for therapeutic intervention, paving the way for novel treatment strategies in ischemic stroke.

Supplementary information.

- Figs. S1 to S9
- Tables S1-S4

Acknowledgements. We thank Wei Qiu and Zhengqi Lu for helpful discussion and technical assistance. This research was supported by grants from the National Key R&D Program of China grants 2022ZD0214300 (C.T.), the National Natural Science Foundation of China grants 82471382 (C.T.), Science and Technology Plan Project of Guangzhou City grants 202201020489 and 2023A04J1089 (C.T.); Special project for the cultivation of the National Natural Science Foundation of the Third Affiliated Hospital of Sun Yat- Sen University(P02567 to H.L.); Guangdong Basic and Applied Basic Research Regional Joint Fund (2023A1515110053 to Y.Y.L.); Medical Scientific Research Foundation of Guangdong Province of China (A2023102 to Y.Y.L.); the National Natural Science Foundation of China grants 82501433(Z.L.)

Declarations

- The authors declare no competing interests.
- Consent for publication was obtained from all individual participants included in the study.
- The data supporting the findings of this study are available from the corresponding author upon reasonable request.
- Author contribution:/Conceptualization: CT, YD; Methodology: CT, YD; Software: Non-applicable; Validation: CT, YAH, HL; Formal analysis: YD, HYL, XM; Investigation: YD, JC, YL; Resources: CT, HL, YAH; Data curation: YD, YBL, DM; Writing - original draft: CT, YD, HL, DM, YBL; Writing - review & editing: CT, YD, GYW; Visualization: CT, YD, DM, XL; Supervision: YH, GW, BJZ; Project administration: CT, YD, HL; Funding acquisition: CT, HL, TL, XL

Ethics Declaration

All animal care and experimental procedures were performed in accordance with the National Institutes of Health (NIH) Guide for the Care and Use of Laboratory Animals and approved by the Institutional Animal Care and Use Committee (IACUC) of Sun Yat-sen University. All human studies were conducted in compliance with the 1964 Declaration of Helsinki and its later amendments or comparable ethical standards, as well as the principles of ICH-GCP, CIOMS, and Chinese GCP. The study was approved by the Medical Ethics Committee of Sun Yat-sen University(RG2023-222-02). Written informed consent was obtained from all individual participants included in the study.

Editorial Policies for:

Springer journals and proceedings: https://www.springer.com/gp/editorial-policies

Nature Portfolio journals: https://www.nature.com/nature-research/editorial-policies

Scientific Reports: https://www.nature.com/srep/journal-policies/editorial-policies

BMC journals: https://www.biomedcentral.com/getpublished/editorial-policies

Appendix A Section title of first appendix

An appendix contains supplementary information that is not an essential part of the text itself but which may be helpful in providing a more comprehensive understanding of the research problem or it is information that is too cumbersome to be included in the body of the paper.

References

[1] Behera, D.K., Rahut, D.B., Mishra, S.: Analyzing stroke burden and risk factors in india using data from the global burden of disease study. Scientific Reports **14**(1), 22640 (2024)

[2] Donkor, E.S.: Stroke in the 21(st) century: a snapshot of the burden, epidemiology, and quality of life. Stroke Research and Treatment **2018**, 3238165 (2018)

[3] Martinez-Coria, H., Arrieta-Cruz, I., Cruz, M.E., López-Valdés, H.E.: Physiopathology of ischemic stroke and its modulation using memantine: evidence from preclinical stroke. Neural Regeneration Research **16**(3), 433–439 (2021)

[4] Alkahtani, R.: Molecular mechanisms underlying some major common risk factors of stroke. Heliyon **8**(8), 10218 (2022)

[5] Rehman, S., Nadeem, A., Akram, U., Sarwar, A., Quraishi, A., Siddiqui, H., Malik, M., Nabi, M., Ul H, I., Cho, A., et al.: Molecular mechanisms of ischemic stroke: a review integrating clinical imaging and therapeutic perspectives. Biomedicines **12**(4) (2024)

[6] Sasannia, S., Leigh, R., Bastani, P.B., Shin, H.G., Zijl, P., Knutsson, L., Nyquist, P.: Blood-brain barrier breakdown in brain ischemia: insights from mri perfusion imaging. Neurotherapeutics **22**(1), 00516 (2025)

[7] Zhao, T., Su, Z., Li, Y., Zhang, X., You, Q.: Chitinase-3 like-protein-1 function and its role in diseases. Signal Transduction and Targeted Therapy **5**(1), 201 (2020)

[8] Mwale, P.F., Hsieh, C.T., Yen, T.L., Jan, J.S., Taliyan, R., Yang, C.H., Yang, W.B.: Chitinase-3-like-1: a multifaceted player in neuroinflammation and degenerative pathologies with therapeutic implications. Molecular Neurodegeneration **20**(1), 7 (2025)

[9] Connolly, K., Lehoux, M., O'Rourke, R., Assetta, B., Erdemir, G.A., Elias, J.A., Lee, C.G., Huang, Y.A.: Potential role of chitinase-3-like protein 1 (chi3l1/ykl-40) in neurodegeneration and alzheimer's disease. Alzheimer's & Dementia **19**(1), 9–24 (2023)

[10] Li, F., Liu, A., Zhao, M., Luo, L.: Astrocytic chitinase-3-like protein 1 in neurological diseases: potential roles and future perspectives. Journal of Neurochemistry **165**(6), 772–790 (2023)

[11] Zhao, H., Huang, M., Jiang, L.: Potential roles and future perspectives of chitinase 3-like 1 in macrophage polarization and the development of diseases. International Journal of Molecular Sciences **24**(22) (2023)

[12] Coffman, F.D.: Chitinase 3-like-1 (chi3l1): a putative disease marker at the interface of proteomics and glycomics. Critical Reviews in Clinical Laboratory Sciences **45**(6), 531–562 (2008)

[13] Rakers, C., Schleif, M., Blank, N., Matůšková, H., Ulas, T., Händler, K., Torres, S.V., Schumacher, T., Tai, K., Schultze, J.L., *et al.*: Stroke target identification guided by astrocyte transcriptome analysis. Glia **67**(4), 619–633 (2019)

[14] Sheng, H., Dang, L., Li, X., Yang, Z., Yang, W.: A modified transcranial middle cerebral artery occlusion model to study stroke outcomes in aged mice. Journal of Visualized Experiments (195) (2023)

[15] Matejuk, A., Ransohoff, R.M.: Crosstalk between astrocytes and microglia: an overview. Frontiers in Immunology **11**, 1416 (2020)

[16] Im, J.H., Yeo, I.J., Park, P.H., Choi, D.Y., Han, S.B., Yun, J., Hong, J.T.: Deletion of chitinase-3-like 1 accelerates stroke development through enhancement of neuroinflammation by stat6-dependent m2 microglial inactivation in chitinase-3-like 1 knockout mice. Experimental Neurology **323**, 113082 (2020)

[17] Russo, C., Valle, M.S., Casabona, A., Malaguarnera, L.: Chitinase signature in the plasticity of neurodegenerative diseases. International Journal of Molecular Sciences **24**(7) (2023)

[18] Vandenbark, A.A., Offner, H., Matejuk, S., Matejuk, A.: Microglia and astrocyte involvement in neurodegeneration and brain cancer. Journal of Neuroinflammation **18**(1), 298 (2021)

[19] Yilmazer-Hanke, D., Ouali, A.N., Fang, L., Klotz, S., Kovacs, G.G., Pankratz, H., Weis, J., Katona, I., Scheuerle, A., Streit, W.J., *et al.*: Differential glial chitotriosidase 1 and chitinase 3-like protein 1 expression in the human primary visual cortex and cerebellum after global hypoxia-ischemia. Neuroscience **506**, 91–113 (2022)

[20] Wiley, C.A., Bonneh-Barkay, D., Dixon, C.E., Lesniak, A., Wang, G., Bissel, S.J., Kochanek, P.M.: Role for mammalian chitinase 3-like protein 1 in traumatic brain injury. Neuropathology **35**(2), 95–106 (2015)

[21] Pinteac, R., Montalban, X., Comabella, M.: Chitinases and chitinase-like proteins as biomarkers in neurologic disorders. Neurology, Neuroimmunology & Neuroinflammation **8**(1) (2021)

[22] Lee, C.M., He, C.H., Nour, A.M., Zhou, Y., Ma, B., Park, J.W., Kim, K.H., Dela, C.C., Sharma, L., Nasr, M.L., *et al.*: Il-13r α2 uses tmem219 in chitinase 3-like-1-induced signalling and effector responses. Nature Communications **7**, 12752 (2016)

[23] Yeo, I.J., Lee, C.K., Han, S.B., Yun, J., Hong, J.T.: Roles of chitinase 3-like 1 in the development of cancer, neurodegenerative diseases, and inflammatory diseases. Pharmacology & Therapeutics **203**, 107394 (2019)

[24] Xu, W., Chao, R., Xie, X., Mao, Y., Chen, X., Chen, X., Zhang, S.: Il13rα2 as a crucial receptor for chi3l1 in osteoclast differentiation and bone resorption through the mapk/akt pathway. Cell Communication and Signaling **22**(1), 81 (2024)

[25] Fan, Y., Meng, Y., Hu, X., Liu, J., Qin, X.: Uncovering novel mechanisms of chitinase-3-like protein 1 in driving inflammation-associated cancers. Cancer Cell International **24**(1), 268 (2024)

[26] Jatczak-Pawlik, I., Jurewicz, A., Domowicz, M., Ewiak-Paszyńska, A., Stasiołek, M.: Chi3l1 in multiple sclerosis-from bench to clinic. Cells **13**(24) (2024)

[27] Mathias, K., Machado, R.S., Andrade, N.M., Piacentini, N., Martins, C.D., Prophiro, J.S., Petronilho, F.: Chitinase-3 like-protein-1 signature in neurological disorders: emphasis on stroke. Journal of Molecular Neuroscience **75**(1), 25 (2025)

[28] Li, J., Li, H., Wang, Y., Zhao, X., Wang, S., Li, L.: Chi3l1 in the csf is a potential biomarker for anti-leucine-rich glioma inactivated 1 encephalitis. Frontiers in Immunology **13**, 1071219 (2022)

[29] Rathcke, C.N., Thomsen, S.B., Linneberg, A., Vestergaard, H.: Variations of chi3l1, levels of the encoded glycoprotein ykl-40 and prediction of fatal and non-fatal ischemic stroke. PLOS ONE **7**(8), 43498 (2012)

[30] Gill, A.J., Schorr, E.M., Gadani, S.P., Calabresi, P.A.: Emerging imaging and liquid biomarkers in multiple sclerosis. European Journal of Immunology **53**(8), 2250228 (2023)

[31] Lucchini, M., De Arcangelis, V., Piro, G., Nociti, V., Bianco, A., De Fino, C.,

Di Sante, G., Ria, F., Calabresi, P., Mirabella, M.: Csf cxcl13 and chitinase 3-like-1 levels predict disease course in relapsing multiple sclerosis. Molecular Neurobiology **60**(1), 36–50 (2023)

[32] Talaat, F., Abdelatty, S., Ragaie, C., Dahshan, A.: Chitinase-3-like 1-protein in csf: a novel biomarker for progression in patients with multiple sclerosis. Neurological Sciences **44**(9), 3243–3252 (2023)

[33] Yu, J.E., Yeo, I.J., Han, S.B., Yun, J., Kim, B., Yong, Y.J., Lim, Y.S., Kim, T.H., Son, D.J., Hong, J.T.: Significance of chitinase-3-like protein 1 in the pathogenesis of inflammatory diseases and cancer. Experimental & Molecular Medicine **56**(1), 1–18 (2024)

[34] Liu, D., Hu, X., Ding, X., Li, M., Ding, L.: Inflammatory effects and regulatory mechanisms of chitinase-3-like-1 in multiple human body systems: a comprehensive review. International Journal of Molecular Sciences **25**(24) (2024)

[35] Yi, L., Li, Z.X., Jiang, Y.Y., Jiang, Y., Meng, X., Li, H., Zhao, X.Q., Wang, Y.L., Liu, L.P., Wang, Y.J., *et al.*: Inflammatory marker profiles and in-hospital neurological deterioration in patients with acute minor ischemic stroke. CNS Neuroscience & Therapeutics **30**(3), 14648 (2024)

[36] Liu, Z., Chopp, M.: Astrocytes, therapeutic targets for neuroprotection and neurorestoration in ischemic stroke. Progress in Neurobiology **144**, 103–120 (2016)

[37] He, L., Zhang, R., Yang, M., Lu, M.: The role of astrocyte in neuroinflammation in traumatic brain injury. Biochimica et Biophysica Acta - Molecular Basis of Disease **1870**(3), 166992 (2024)

[38] Cekanaviciute, E., Buckwalter, M.S.: Astrocytes: integrative regulators of neuroinflammation in stroke and other neurological diseases. Neurotherapeutics **13**(4), 685–701 (2016)

[39] Li, K., Li, J., Zheng, J., Qin, S.: Reactive astrocytes in neurodegenerative diseases. Aging and Disease **10**(3), 664–675 (2019)

[40] Lawrence, J.M., Schardien, K., Wigdahl, B., Nonnemacher, M.R.: Roles of neuropathology-associated reactive astrocytes: a systematic review. Acta Neuropathologica Communications **11**(1), 42 (2023)

[41] Li, J., Zheng, M., Shimoni, O., Banks, W.A., Bush, A.I., Gamble, J.R., Shi, B.: Development of novel therapeutics targeting the blood-brain barrier: from barrier to carrier. Advanced Science **8**(16), 2101090 (2021)

[42] Archie, S.R., Al, S.A., Cucullo, L.: Blood-brain barrier dysfunction in cns disorders and putative therapeutic targets: an overview. Pharmaceutics **13**(11)

(2021)

[43] Soares, L.C., Al-Dalahmah, O., Hillis, J., Young, C.C., Asbed, I., Sakaguchi, M., O'Neill, E., Szele, F.G.: Novel galectin-3 roles in neurogenesis, inflammation and neurological diseases. Cells **10**(11) (2021)

[44] Mijailović, N.R., Vesic, K., Arsenijevic, D., Milojević-Rakić, M., Borovcanin, M.M.: Galectin-3 involvement in cognitive processes for new therapeutic considerations. Frontiers in Cellular Neuroscience **16**, 923811 (2022)

[45] Liang, T., Zhu, Z., Gong, F., Yang, X., Lei, X., Lu, L.: Galectin-3 promotes brain injury by modulating the phenotype of microglia via binding tlr-4 after intracerebral hemorrhage. Aging **15**(17), 9041–9058 (2023)

[46] García-Revilla, J., Boza-Serrano, A., Espinosa-Oliva, A.M., Soto, M.S., Deierborg, T., Ruiz, R., Pablos, R.M., Burguillos, M.A., Venero, J.L.: Galectin-3, a rising star in modulating microglia activation under conditions of neurodegeneration. Cell Death & Disease **13**(7), 628 (2022)

[47] Ahmed, R., Anam, K., Ahmed, H.: Development of galectin-3 targeting drugs for therapeutic applications in various diseases. International Journal of Molecular Sciences **24**(9) (2023)

[48] Lee, Y.S., Yu, J.E., Kim, K.C., Lee, D.H., Son, D.J., Lee, H.P., Jung, J.K., Kim, N.D., Ham, Y.W., Yun, J., *et al.*: A small molecule targeting chi3l1 inhibits lung metastasis by blocking il-13r α2-mediated jnk-ap-1 signals. Molecular Oncology **16**(2), 508–526 (2022)

[49] Holloway, P.M., Gavins, F.N.: Modeling ischemic stroke in vitro: status quo and future perspectives. Stroke **47**(2), 561–569 (2016)

[50] Bryniarska-Kubiak, N., Kubiak, A., Trojan, E., Wesołowska, J., Lekka, M., Basta-Kaim, A.: Oxygen-glucose deprivation in organotypic hippocampal cultures leads to cytoskeleton rearrangement and immune activation: link to the potential pathomechanism of ischaemic stroke. Cells **12**(11) (2023)

[51] Fluri, F., Schuhmann, M.K., Kleinschnitz, C.: Animal models of ischemic stroke and their application in clinical research. Drug Design, Development and Therapy **9**, 3445–3454 (2015)

[52] Zeng, L., Hu, S., Zeng, L., Chen, R., Li, H., Yu, J., Yang, H.: Animal models of ischemic stroke with different forms of middle cerebral artery occlusion. Brain Sciences **13**(7) (2023)

[53] Hong, P., Gu, R.N., Li, F.X., Xiong, X.X., Liang, W.B., You, Z.J., Zhang, H.F.: Nlrp3 inflammasome as a potential treatment in ischemic stroke concomitant with diabetes. Journal of Neuroinflammation **16**(1), 121 (2019)

[54] Puleo, M.G., Miceli, S., Di Chiara, T., Pizzo, G.M., Della, C.V., Simonetta, I., Pinto, A., Tuttolomondo, A.: Molecular mechanisms of inflammasome in ischemic stroke pathogenesis. Pharmaceuticals **15**(10) (2022)

[55] Zhou, Y., He, C.H., Yang, D.S., Nguyen, T., Cao, Y., Kamle, S., Lee, C.M., Gochuico, B.R., Gahl, W.A., Shea, B.S., *et al.*: Galectin-3 interacts with the chi3l1 axis and contributes to hermansky-pudlak syndrome lung disease. Journal of Immunology **200**(6), 2140–2153 (2018)

Supplementary Files

This is a list of supplementary files associated with this preprint. Click to download.

- GraphicalAbstract.tif
- SupplementaryFilev2.pdf